DIRECTED CELL MIGRATION INDUCED BY MULTIPLE CUES IN THE ENGINEERED MICROENVIRONMENT

by

Hye-ran Moon

A Dissertation

Submitted to the Faculty of Purdue University

In Partial Fulfillment of the Requirements for the degree of

Doctor of Philosophy

School of Mechanical Engineering

West Lafayette, Indiana

August 2020

THE PURDUE UNIVERSITY GRADUATE SCHOOL
STATEMENT OF COMMITTEE APPROVAL

Dr. Bumsoo Han
School of Mechanical Engineering

Dr. Andrew Mugler
Department of Physics and Astronomy

Dr. Jong Hyun Choi
School of Mechanical Engineering

Dr. Steven T Wereley
School of Mechanical Engineering

Approved by:
Dr. Nicole L. Key

Dedicated to my beloved family

ACKNOWLEDGMENTS

This dissertation wouldn't have been out without the invaluable advice of my committee members and support from my dear friends and family.

First of all, I would like to acknowledge my advisor, Prof. Bumsoo Han, for giving me an excellent opportunity to pursue a meaningful research experience. His guidance, support, and patience encouraged me to learn more and helped me to successfully complete this dissertation. I would also like to thank the other committee members, Prof. Andrew Mugler, Prof. Jong Hyun Choi, and Prof. Steven T Wereley, for their worthy feedbacks in shaping the research projects and dissertation. Specifically, I am sincerely grateful to Prof. Mugler for sharing his knowledge and giving me meaningful guidance throughout our collaborations. It is no exaggeration to say that I would have missed out on many lessons of knowledge as well as how to communicate and work together without the collaboration with Prof. Mugler, Dr. Julien Varennes, Soutick Saha. Including all the other collaborators, I appreciate everything from them.

I would also like to express many thanks to both current and former members of Biotransport Phenomena Lab (BPL) for their valuable insights for the research as well as friendships. Those memorable fun times that we shared made my graduate life so meaningful and enjoyable. In particular, I would like to thank Dr. Altug Özçelikkale and Mike Bradney, who have been my mentors and friends from the first year at Purdue. Also, I thank Stephanie Venis and Victoria Noe-Kim. Their kind and thoughtful friendships enabled me to successfully adjust the graduate life at Purdue and learn lots of things as a researcher, an engineer, and an individual.

I cannot find sufficient words to express my appreciation to dear my friends enough. I could get all the delightful memories at Purdue especially thanks to them. I also want to thank my parents and brothers for their endless support and encouragement. Specifically, I always feel loved and supported thanks to my beloved baby brother, Jeongwoo Moon.

Finally, I would like to express my deepest gratitude to my fiancé, Byunghoon Ryu, for giving me countless love and companionship for many years. Without him, I wouldn’t have even started any of the work successfully. His love and support indeed enabled this dissertation completed. Beyond the graduate study, he inspires and encourages me whatever I would like to achieve as myself. I am excited by our future we will go through together.

TABLE OF CONTENTS

LIST OF FIGURES

ABSTRACT

Directed cancer cell migration induced by the environmental signals is a critical process in cancer metastasis. Cancer cells are exposed to complex chemical and mechanical signals stimulating directed migration in the tumor microenvironment, where the physical nature is highly complex. It is still barely understood how cells sense and process the complex environmental signals through the complex intercellular signaling networks to execute the cell responses. This study explores the migratory response of cancer cells under a single and combined signal. The driving hypothesis is that the cell innate capability constraints the signal stimulations physically in inducing directed cell migration. We assess the hypothesis by engineering the microenvironment in the microfluidic platform, exposing a single or combined signal environment. The combined signal environment is established by 1) two different chemoattractants (TGF-β1 and EGF) and 2) the convection-driven signal environment (TGF-β1 and interstitial flow). The results show that the performance of cancer cell directed migration is physically constrained when the environmental stimulation meets the cell's innate physical limit. We illustrate the results in a physical and quantitative manner. This approach provides a novel insight to understand the cellular process and eventually enables to predict the cellular response under the complex environmental signals.

1. INTRODUCTION

Directed cell migration is a phenomenon that plays a central role in various physiological and pathological processes, including cancer metastasis, organism development, immune system function, wound healing, and embryogenesis [1-7]. Specifically, directed cell migration is a crucial step in cancer metastasis, and it is a major cause of cancer-related death [8-10]. For decades, cell migratory behaviors have been largely understood by elucidating the interactions between cells and relevant regulators. In the tissue microenvironment, cells encounter multiple environmental components, including the extracellular matrix (ECM), interstitial fluid, and various soluble factors [11-15]. These components are crucial in regulating physiological cell functions involving nutrient transport to regulate cell survival, homeosis, and fate. In contrast, the cancer microenvironment has distinct features. Upregulated growth factors and chemokines are secreted by desmoplastic stroma. The tissue is highly stiff with dense stroma and abundant ECM components. The leaky vasculature and stiff tissue increase interstitial fluid pressure, which causes the local pressure gradient. By interacting with the environmental cues in such a complex environment, cancer cells show distinct features in their locomotion [8, 13-22].

Recent studies investigating the cell response to a specific cue have shown that relevant environmental cues promote directional cell migration [4, 14-26]. *Chemotaxis* is the directed cell migration induced by chemical gradients. Growth factors and chemokines, such as endothelial growth factor (EGF), transforming growth factor-β (TGF-β), colony stimulating factor1 (CSF1), CXCL12 (also known as SDF1α), and CCL19 have been reported as chemoattractants that induce chemotaxis in cancer. Most of these soluble factors induce chemotaxis through intracellular signaling cascades which regulate the cell polarization involved in cytoskeletal dynamics. Recent studies demonstrated that the motility of breast cancer cells induced by an EGF gradient was enhanced, while their migration directions were highly biased [25, 26]. The binding of EGF and EGFR is known to trigger the cofilin pathway, which regulates the structural basis of actin filaments [27, 28]. Interstitial flow is also a regulator that induces directed cell migration, called *rheotaxis*. Polacheck, et al. [29] investigated the effect of interstitial flow on the movement of breast cancer cells, showing that the direction of their movement is aligned to the flow streamline and is biased toward either the upstream or downstream direction of the flow depending on the

specific circumstance [29]. Further, the flow-induced migration has been recognized as a cell response to autologous chemotaxis or focal adhesive kinases (FAK) pathways.

Despite recent advances in the identification of environmental cues inducing directed cell migration and relevant signaling pathway cascades, the way in which cells process and respond to environmental signals remains unclear. Specifically, cancer cell locomotion in highly complex and heterogeneous microenvironments is not well understood. The tissue microenvironment is highly complex and is composed of multiple environmental cues, such as growth factor, interstitial flow, and ECM, which co-exist and affect each other's reactions. To overcome this barrier, it is important to study cell response to multiple co-existing cues and the mechanism behind their combined effect on cell migration.

The cell chemotactic performances are a systematic response to co-existing and cross-effecting multiple cues as well as cell capability in signal processing for sensing and responding to the cues. In this study, the migratory cell behaviors induced by multiple cues are investigated in an engineered *in vitro* microenvironment. The migratory behaviors represented by motility and directional performances show a resultant balance of extrinsic and intrinsic processes in the directed cell migration. In this sense, we hypothesize that the cell's innate capability of signal processing physically governs cell response after sensing the cues.

Initially, we investigated migratory cell behaviors with a single cue, TGF-β gradient, to elucidate the physical relations between the directional accuracy and persistence of cell migration. In this study, we investigated the physical constraints of the chemotactic performance of breast cancer cells using a 3-dimensional (3D) *in vitro* gradient platform. This study showed the physical limits of chemotactic performance in the accuracy–persistence space, indicating that the movement features in response to a chemical gradient are physically limited due to the cell's innate sensing and responding capabilities. Next, we studied the cell migration induced by the combined signals of TGF-β and EGF gradients. The combined chemical-signal environment was engineered in an *in vitro* chemotaxis platform to determine how the cell's innate capability of processing signals affects directional accuracy in the multiple signal environment. Interestingly, we observed an antagonistic effect of the combined gradients of TGF-β and EGF, which are recognized as synergistic promoters of cell migration ability [30]. We illustrated the result by proposing a simple mathematical model describing a downstream common signal molecule, which takes charge in regulating directed cell migration. We hypothesized that the limited number of common molecules

determines the cell's innate processing capability, delineating the bias behavior in the cell migration when the common molecules are saturated. We tested the hypothesis with predictable scenarios by applying higher background concentrations of either TGF-β or EGF. Finally, we considered a cell response to the complex signal environment involved in both chemical and shear flow stimulation. We found that the flow stimulation induces directed cell migration in the upstream direction of the flow, excluding additional chemical signals. Meanwhile, the flow alters the chemical environment, contributing to the soluble factor transport in the microenvironment. We evaluated the effect of such a complex environment on the directed cell migration of pancreatic cancer cells by hypothesizing that the flow signal shares the common downstream molecules to regulate the cell migratory response. The complex signal environment was decoupled by estimating the physical detection limit of the cells in the shallow gradient. Overall, these studies provide new insights for understanding the cellular process in directed migration based on physical and quantitative approaches involving the implementation of a controllable engineered microenvironment.

2. LITERATURE REVIEW

2.1 Intrinsic capability of cells in directed cell migration

Directed cell migration is a cell response by interacting with microenvironmental cues. In the interaction between cells and microenvironmental signals, the cell sensory capability is a primary step. The sensing capability for chemical cues is relevant to the molecules' binding to receptors on the cells [31-35]. Cells also have the ability to sense mechanical cues through their adhesion dynamics with the ECM [36-41]. Such sensing processes result in intrinsic signaling pathways to either activate or suppress specific protein molecules to regulate cells' intrinsic functions [4, 34]. The signaling steps have highly intricate correlations with each other. As a result of the complex signaling transductions, the cells are polarized ,having leading and trailing edges that play distinct roles in driving motility and directionality of the cell movement [4, 17, 18, 34]. In this section, the intrinsic capability of the cell to sense and respond to the cue is briefly reviewed to study intrinsic mechanism of the directed migration.

2.1.1 Cell capability to sense a cue

In the process of the directed cell migration, cells initially sense the cues in the microenvironment, then respond to the cue in polarization and migration. [4, 34] For chemotaxis, cells sense a concentration gradient of growth factors. Theoretically, a eukaryotic cell, whose size is relatively large at 10-20um in diameter, can sense the gradient of cues by sensing the concentration difference between the spatial ends.[34] Receptors can determine the cells' sensing capability on the cell membrane, geometry of the cells, and molecule dispersion near the cells [31, 33]. A remarkable aspect of the sensing capability of the cells is the gradient [33]. The relative change of the molecule gradient is defined as a change in concentration across the body divided by a background concentration. Eukaryotic cells generally can sense shallow gradient signals in the microenvironment as small as 2-10% between the cells' endpoints.[32-34] The sensory precision has been similarly shown in simple amoebae such as *Dictyostelium discoideum* (*D. discoideum*), tumor cells, and neutrophils. The simple model has been used for signaling pathways inducing chemotaxis [4, 34, 42]. Several studies have driven the physical limits of the sensory precision theoretically by using the physics of molecule counting [32, 33, 43, 44]. Chemotactic

accuracy measurement of *D. discoideum* has shown that sensory precision is remarkably close to the physical limit (1%-5%) [31].

2.1.2 Molecular networks in the directed cell migration

Once the cells sense the cue, several molecular signaling cascades occur in the cells to trigger its function in directed migration and polarization. The molecular signaling pathways involved in directed cell migration are mostly related to cytoskeleton dynamics, which can regulate the direction of cell movement and serve as the driving force in cell motility [4, 34, 45, 46]. For example, the signaling through receptors for chemokines, a G protein-coupled receptor (GPCR), or growth factor receptors, a receptor tyrosine kinases (RTK), has been widely studied showing influence on the initial protrusion required in the directed cell migration. [4, 34]. Either molecular binding through GPCR/RTK or adhesion of integrins to the ECM leads to the activation of RHO GTPases. The RHO GTPases functions to control actin polymerization within the leading-edge protrusion, which plays a vital role in the directed migration[4, 34, 42]. In tumor chemotaxis, the EGF gradient is relevant in signaling in mammary tumors showing directed pseudopods [27, 47]. Arp 2/3 complex signaling is also related [4, 34, 46, 48]. cGMP in neutrophil and ROCK signaling pathways are relevant to localizing myosin filaments[4, 34, 45, 46, 49]. The combined activities from those signaling cascades are involved in cell polarization and retraction of the rear of the cells contributing to directed migration.

D. discoideum has been used as a simple model to study signaling pathways related to chemotaxis [4, 34, 42]. The studies using *D. discoideum* have impacted on the investigation of GPCR signaling pathways controlling chemotaxis in many other cell types, including tumor cells and neutrophils. Signaling pathways carrying Phosphatidylinositol 3-kinase (P13K) and protein kinase B (PKB, also known as Akt) lead to enhancement of actin polymerization and pseudopod formation showing filamentous (F)-actin filled pseudopodia, which helps in creating cell polarity during cell migration [4, 34, 50-52].

2.2 Tissue microenvironment

The extracellular microenvironment plays an essential role in directed cell migration. It provides diverse signals regulating the movement of the cells [6, 7, 17]. It provides environmental cues as well as the ECM components that physically constraint the cell movement. In chemotaxis,

chemoattractants secreted from the interstitial region (interstitium) are exposed to the cells as the concentration gradient in the microenvironment [4]. Also, ECM components in the microenvironment physically interact with cells. Different features in the ECM, such as pore size and degree of adhesion between cells and ECM, shift the modes of cell migration. [19, 53] The cell migration results from a balance between intrinsic and extrinsic regulators; therefore, it is crucial to understand how environmental conditions interact with the cells. In this section, we briefly review the characteristics of ECMs and interstitial flow affecting cell migration behaviors.

2.2.1 Extracellular matrix and cell migration

Cells sense the environmental cues and respond through relevant signaling pathways. The cell migratory response varies to directed migration, biased protrusion, or random walk. The modes of cell migration are determined by the surrounding microenvironment and the cells' capability. Extracellular matrix (ECM) is one of the major components in the tissue microenvironment [4, 7, 17, 54, 55]. ECM is a porous matrix composed of collagen, elastin, and proteoglycan [11]. It provides adhesive points essential in cell migration and also plays a role in physically constraining the cell movement [17, 39, 41, 56]. As the ECM is denser and stiffer, it is challenging for the cells to have motility. In the high constraint condition, cells need to degrade the matrix by applying the enzymatic process with matrix metalloproteinases (MMPs). The threshold to govern cell migration through the matrix has been recognized as a 'nuclear limit'. When the matrix pore size is less than ~10% of the cross-sectional nuclear size, cells capable of moving without MMPs. [17, 18]. Depending on the adhesion of extracellular matrix with cells, motile-characteristics of cells can be classified in amoeboid migration of mesenchymal migration [4, 17, 18]. Interestingly, ECM could induce directed cell migration. [15, 17, 23, 29, 57] Mechanical signals such as a stiffness gradient developed in the ECM are environmental cues regulating directed cell migration [20, 21, 41]. In cancer, ECM has a distinct architecture, which contributes to cancer metastasis. ECM architectures are reorganized by malignant stromal cells such as CAFs, consequently, develop a confined highway for the cancer cell invasion. [4, 17]

2.2.2 Interstitial flow in tissue microenvironment

Tissues in our body system are filled with interstitial fluid. The interstitial fluid plays a crucial role in physiology by transporting various molecules and gases [13]. Nutrition can be

delivered from the blood vessel to cells through interstitial fluid perfusion. In addition to nourishment, chemical cues, and various proteins to induce physiological processes such as angiogenesis, embryogenesis, and tumor metastasis are transported in the interstitial fluid [13, 14, 41]. The interstitial fluid is not stationary, but it flows in the microenvironment due to pressure differences. In the circulatory system, plasma is leaked from blood vessels by Starling's law and the osmotic pressure difference and is perfused to the interstitial fluid [13]. Near the interstitium, the interstitial fluid containing waste can be similarly drained to lymphatics. This circulatory process generates the pressure gradient in the interstitium by transvascular fluid transport. Besides, diverse factors induce interstitial fluid pressure (IFP), including body movement, tissue metabolism, hydration, ECM composition, and cell density [11, 13]. In the tumor microenvironment, it has been reported that higher IFP occurs due to leaky vasculature and pressured lymphatics due to abnormally grown cell density and malignant ECM components. In the chemotaxis, the transport of chemical cues from their secreting site or blood vessel is a fundamental step to develop a gradient of the cue [11, 14, 18, 23, 24, 54]. Therefore, it is essential to understand the physical principles of solute transport in the interstitium considering the interstitial fluid flow.

2.2.3 Physics of mass transport in tissue microenvironment

In many cases, soluble factors, a key regulator in the chemotaxis, are secreted by stromal cells to function as a signal to guide cell movement in the microenvironment. Althernatively, chemotaxis could occur by the gradient of components such as soluble factors, nutrients, and oxygen transported by the blood vessel. The chemical cues are transported to an interstitium based on the concentration difference from the secreting point. In the process in which the molecules reach the target cells by the diffusion principle, a spatiotemporal concentration gradient can be developed naturally in the microenvironment. Cells sense the gradient present in the microenvironment and show directed cell migration where the movement is guided. Such chemical gradient development in the microenvironment can be addressed by formulating some governing equations. However, the microenvironment is highly heterogeneous, depending on tissue type. To simplify the problem, the theoretical illustrations in this section focus on tumor microenvironments with remarkable features of the solid tumor, given that theoretical basics should be applicable to other tissue microenvironments.

The transport phenomenon in the interstitium can be explained by the conservation laws of the fluid and solute in porous materials[11, 13, 58]. The interstitium is composed of various ECM components with cells, and the pore space is filled with interstitial fluid. Considering porosity ϕ and the deformation of the porous material with $\vec{u}$, mass conservation is governed by the following equation:

$$\nabla \cdot \left\{ \phi v_f + (1-\phi) \frac{\partial \vec{u}}{\partial t} \right\} = Q_v - Q_d$$

where v_f indicates flow rate, Q_v is flow rate across the vessel per unit tissue volume, and Q_d is the flow rate across the lymphatic (drain) per unit tissue volume.

The momentum conservation of the interstitial flow is introduced with Darcy's law which is applicable when the flow is highly slow, and flow-matrix is not interacting:

$$\phi(v_f - \frac{\partial \vec{u}}{\partial t}) = -\frac{K}{\mu} \nabla p_i$$

Following by the fluid, the solute can be governed by mass conservation:

$$\frac{\partial C}{\partial t} = -\nabla \cdot N + (\Phi_v - \Phi_d) + R$$

where the mass flux N is defined as:

$$N = -D_{eff} \cdot \nabla C + v_f \cdot C$$

The solute source from the vessel can be expressed with Kedem-Katchalsky formulation, which addresses mass conservation in transvascular transport of the solute from blood vessels:

$$\Phi_v = Q_v (1-\sigma_s) \overline{C_s} + \frac{PS}{V} (C_p - \frac{C}{K_{av}})$$

Although we can assume the coefficients and properties as the constant values, they are sometimes strongly dependent on tissue structure as well as binding kinetics of relevant soluble cues. For example, the effective diffusivity is determined by many aspects, including particle size, surface condition, structure porosity, and temperature [58]. Likewise, hydraulic conductivity is temperature-dependent since it contains a fluid viscosity term. ECM components such as glycosaminoglycan could also affect K [58]. Therefore, the transport of chemical factors can be tissue type- or patient-dependent.

2.3 Methodologies to study directed cell migration

Recent studies have identified the cell sensing capabilities and various extracellular regulators affect chemotaxis. However, the mechanism to link the functions of intrinsic characteristics and extracellular regulators is still elusive due to the inherent complexity of the process. In this section, we review several models to approach the research question of how the cells interact with the microenvironment and respond in the directed migration. As emphasizing the importance of the chemotactic behavior of cells cultured in 3D conditions, various *in vitro* systems are illustrated from conventional methods to recent advances by using micro-fluidics.

2.3.1 Physical models

Biophysical models studying the directed cell migration have advanced our understanding of the directed cell migration's mechanistic insight. In the physical models, sensory dynamics can be illustrated in physical ways, which enables the description of the sensory capability of cells. Physical limits on cell gradient sensing capability have been addressed by using receptor-molecular binding dynamics. [32, 33] Moreover, how cells process the signal and result in the directed movement can be approached with physical models in the quantitative matter. Relevant molecular mechanisms have illustrated how signaling transduction work to promote the directed cell movement. However, the intricate biological processes through molecular networks are highly complex and have a limitation in elucidating the quantitative mechanisms of the directed cell migration. [33] In this respect, the local excitation global inhibition (LEGI) model has described a spatial regulation of cofilin activity, which is a signaling pathway relevant to local actin polymerization in leading-edge protrusions [4, 27, 33-35]. The model focuses on a link between the sensing process and responding to the cue by expressing the localization of cofilin in the model.

Following the studies regarding cell sensing and the link of cell sense to response, physical models have been established to describe physical and mechanical interactions during cell migration. Initially, the random cell movement in the cells cultured in 2D was illustrated by a random walk model, a stochastic process to determine its path [59]. The random walk model describes cell migration as the most efficient way to move. Although it has addressed the random cell migration well, cell locomotion shows directional characteristics interacting with the microenvironment. Random walk motion has been further expanded to a biased persistence random walk model (BPRW), including directional bias and persistence terms [60-62].

2.3.2 *In vitro* models

For a long time, biological interpretations to illustrate cell behaviors have been developed by culturing the cells on two-dimensional (2D) plastic substrate or glass. However, cells in the actual *in vivo* microenvironment are surrounded by highly heterogeneous conditions with ECM components and various stromal cells [23]. Since cell migration is a phenomenon caused by interaction with the complex environment, there is a limitation in the 2D model [15, 23]. To capture the microenvironment close to real, in vivo platform is widely used. However, it is not easy to control the environmental factors *in vivo* platform. Moreover, *in vivo* studies are considerably expensive and inefficient in time. To overcome such barriers, many studies in cell biology have been developed three-dimensional (3D) *in vitro* platforms to capture the complex microenvironment by using microfluidics. In this chapter, the recent advances in 3D *in vitro* platform for the directed cell migration are reviewed.

Several conventional methods have been successfully applied in chemotaxis to identify relevant chemoattractants and their molecular mechanism. Transwell assay (also called Boyden chamber) developed by Boyden in 1962 [63] has mimicked the process of cell transvascular transport by sitting the cell suspension on a filter membrane in between fresh medium on top and chemoattractant solution on the bottom. Several 2D assays, including scratch wound healing, have been applied to distinguish whether the cells are affected by a chemoattractant or not [4, 15, 23]. To investigate the cell migratory characteristics and the cell polarity, micropipette assay has also been used [4, 64-66]. Recently, research advances in engineering micro-fluidics allow acute control of the cell surrounding environment. Cell migration in response to a chemical gradient has been investigated with T-junction or dilution network micro-fluidics which are flow-driven 2D spatial gradient chamber [11, 67-73]. Also, several conventional methods were further developed by micro-fluidics having better control to reveal chemoattract characteristics of soluble factors by counting cells affected by the cue.

Although these methods have contributed to advances in understanding relevant chemoattractants and their molecular mechanism, most of them are unable to adequately describe the migratory behaviors of cells stimulated by the chemoattractant due to the absence of ECM components. The migration is a resultant motion by interacting with the surrounding environment [15, 23]. Indeed, cell morphology during migration in 2D showed wide and thin pseudopods, whereas 3D migrating morphology is highly dependent on environmental constraints such as

adhesion, matrix pore size, and stiffness [15, 23]. In this sense, microfluidics started to contain ECM components, including type I collagen, matrigel, and several engineered hydrogels [23, 74-76]. The 3D microfluidics is widely applied to execute the chemotactic performance of cells by using the diffusion principle. [4, 15, 54, 67].

3. PHYSICAL CONSTRAINTS ON ACCURACY AND PERSISTENCE DURING CELL CHEMOTAXIS

3.1 Introduction

Chemotaxis plays a crucial role in many biological phenomena such as organism development, immune system targeting, and cancer progression.[4, 33, 77, 78] Specifically, recent studies indicate that chemotaxis occurs during metastasis in many different types of cancer.[4, 9, 18, 26, 79, 80] At the onset of metastasis, tumor cells invade the surrounding extracellular environment, and oftentimes chemical signals in the environment can help direct the migration of invading tumor cells. Several recent experiments have quantified chemotaxis of tumor cells in the presence of different chemoattractants [78] and others have been devoted to the intracellular biochemical processes involved in cell motion [61]. Since the largest cause of death in cancer patients is due to the onset of metastasis, it is important to understand and prevent the directed and chemotactic behavior of invading tumor cells.

Chemotaxis requires sensing and motility, and a cell's ability to execute these aspects of chemotaxis determines its performance. High chemotactic performance can be defined in terms of several properties. Cell motion should be accurate: cells should move in the actual gradient direction, not a different direction. Cell motion should be persistent: cells should not waste effort moving in random directions before ultimately drifting in the correct direction. Cell motion should be fast: cells should arrive at their destination in a timely manner.

Indeed, most studies of chemotaxis use one or more of these measures to quantify chemotactic performance. Accuracy is usually quantified by the so-called chemotactic index (CI), most often defined in terms of the angle made with the gradient direction [44, 52, 81, 82] although occasionally it is defined in terms of the ratio of distances traveled [83] or number of motile cells [84-86] in the presence vs. absence of the gradient. Persistence is usually quantified by the so-called chemotactic ratio (CR; also called the McCutcheon index[87], length ratio[60], or straightness index [59]), defined as the ratio of the magnitude of the cell's displacement to the total distance traveled by the cell; although recent work has pointed out advantages of using the directional autocorrelation time[48, 60]. Speed is usually quantified in terms of instantaneous speed along the trajectory or net speed over the entire assay.

However, the relationship among the accuracy, persistence, and speed in chemotaxis, and whether one quantity constrains the others, is not fully understood. Are there cells that are accurate but not very persistent, or persistent but not very accurate? If not, is it because such motion is possible but not fit, or is it because some aspect of cell motion fundamentally prohibits this combination of chemotactic properties?

Here we focus on how a cell's intrinsic migration mechanism as well as properties of the external environment place constrains on its chemotactic performance. The physics of diffusion places inherent limits on a cell's ability to sense chemical gradients[88]. There limits, along with the cell's internal information processing and its motility mechanism, determine the accuracy, persistence, and speed of migration. Using a human breast cancer cell line (MDA-MB-231) embedded within a 3D collagen matrix inside a microfluidic device imposing a chemical gradient, we are able to quantify the chemotactic performance of invasive cancer cells in response to various chemical concentration profiles. Results from chemotaxis assays are then compared with simulations and theoretical predictions in order to probe the physical limits to chemotaxis.

3.2 Materials and methods

3.2.1 Cell culture and reagents

Human breast adenocarcinoma cells (MDA-MB-231) were cultured in Dulbecco's Modified Eagle Medium/Ham's F-12 (Advanced DMEM/F-12, Lifetechnologies, CA, USA) supplemented by 5% v/v fetal bovin serum (FBS), 2 mM L-glutamine (L-glu), and 100 μg/ml penicillin/streptomycin (P/S) for less than 15 passages. MDA-MB-231 cells were regularly harvested by 0.05% trypsin and 0.53mM EDTA (Lifetechnologies, CA, USA) when grown up to around 80% confluency in 75 cm^2 T-flasks at 37 ºC with 5% CO_2 incubation. Harvested cells were used for experiments or sub-cultured.

Cell-matrix composition was prepared in the microfluidic device. For the composition, MDA-MB-231 cells were mixed with 2 mg/ml of type I collagen (Corning Inc., NY, USA) mixture prepared with 10X PBS, NaOH, HEPE solution, FBS, Glu, P/S, and cell-culture level distilled water after centrifuged with 1000 rpm for 3 minutes. The cell mixture was filled in center-channel of the microfluidic devices and incubated in at 37 ºC with 5% CO_2. The cells in the collagen matrix were initially cultured in basic medium (DMEM/F12 supplemented by 5% v/v FBS, 2 mM L-glu,

and 100 μg/ml of P/S) for 24 hours. Then the cells were exposed by reduced serum medium for another 24 hours, which was advanced DMEM/F12 containing 1% v/v FBS, 2 mM L-glu, and 100 μg/ml P/S. After 24 hour-serum starvations, cells were exposed by a gradient of transforming growth factor beta-1 (TGF-β1, Invitrogen, CA, USA).

3.2.2 Microfluidic device for chemical gradient

The microfluidic device was designed to generate a linear gradient of soluble factors. The device is composed of three channels which are 100μm in thickness as described previously A center channel that is 1mm wide aims to culture tumor cells with ECM components. The center channel is connected to two side channels. The 300μm-wide side channels are connected to large reservoirs at the end ports including culture medium. Since the side channels are in contact with the top and bottom sides of the center channel, the growth factor gradient can be generated by diffusing the soluble factor from one of the side channels, a source channel, to the other, a sink channel. Assuming there is neither pressure difference nor flow between the side channels, the concentration of a given factor can be described by the chemical species conservation equation as follows:

$$\frac{\partial C}{\partial t} = \nabla \cdot (D_{ab} \cdot \nabla C)$$

Once the concentration profile in the center channel reaches steady state, the linear profile persists for a while and can therefore be approximated by assuming the boundary conditions of concentration at the side channels are constants. To verify the diffusion behavior, the gradient formation was examined by using 10k Da FITC-fluorescence conjugated dextran (FITC-dextran). FITC-dextran solution was applied in the source channel while the sink channel was filled with normal culture medium. The FITC-dextran concentration profile was evaluated by the FITC fluorescent intensity in the center channel. To disregard the effect of photo-bleaching on the results, the intensity was normalized by the intensity of the source channel. The normalized intensity was reasonably considered since the fluorescence intensity of the source channel consistently remained as maximum due to the large reservoirs. The FITC dextran intensity profile showed that the linear profile was developed within 3hours after applying the source and continued for more than 9 hours.

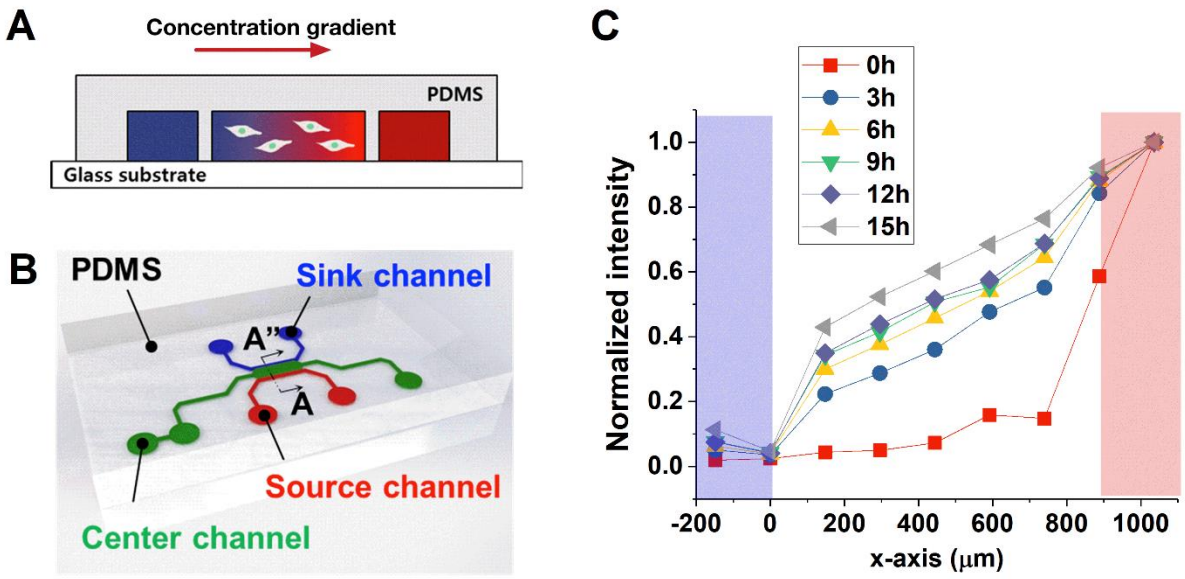

Figure 3.1. Microfluidic device used as a chemotaxis platform. (A) Cross-sectional view illustrating concentration gradient formed by diffusion. (B) Illustration showing structure of the microfluidic channels. Center channel (green) is filled with type I collagen mixture and MDA-MB-231 mixture, source channel is filled with culture medium containing TGF-β, and sink shannel is filled with only culture medium. (C) FITC-dextran fluorescence within the center channel. Blue region indicates sink channel while region indicates source channel.

3.2.3 Characterization of cell migration with time-lapse microscopy

Cell behaviors were captured every 15 minutes for 9 hours using an inverted microscope (Olympus IX71, Japan) equipped with a stage top incubator as described previously, so that the microfluidic platform could be maintainted at 37ºC in a 5% CO2 environment during imaging. The time-lapse imaging was started 3 hours after applying TGF-b1 solution in the source channel to have sufficient adjusting time. To analyze each cell behavior, a cell area in the bright field images were defined by a contrast difference between the cells and a background, and the images were converted to monochrome images by using ImageJ. Cell trajectories were demonstrated by tracking centroids of the cell area. In tracking the cell movements, cells undergoing division were excluded to avoid extra influences to affect cell polarity. Moreover, stationary cells due to the presence of the matrix were excluded. The stationary cells were defined as the cells that moved less than their diameter. A migration trajectory was defined by connecting the centroids of a cell from each time point.

3.2.4 Statistical analysis of experiments

In examining the chemotactic characteristics of each group, more than 40 cell trajectories were evaluated per a group. A data point in Figure 3.3 C-E indicates each metric of a cell trajectory showing distribution characteristics with a box plot. The box plot includes boundaries as quadrants and a center as a median. The distribution of each metric was statistically analyzed by using Mann-Whitney U-test. This non -parametric method was used since the distribution was not consistently normal (the CI is a function of cosine). The significant change on the population lies on the biased distribution of each cell parameter when $p<0.05$. Futrthermore, the experiments were repeated at least 3 times and reported with means of medians ± standard estimated error (S.E.M) in Figure 3.4. To evaluate physical limits on each metric, the data points were compared each other using a student t-test. The statistical significance between comparisons were examined when $p<0.05$.

3.3 Results

3.3.1 Quantifying directional accuracy, persistence, and speed

We measure directional accuracy using the chemotactic index (CI) [44, 52, 81, 82]

$$\mathrm{CI} \equiv \langle \cos\theta \rangle$$

where θ is the angle the cell's displacement makes with the gradient direction (Figure 3.2), and the average is taken over many cell trajectories. CI is bounded between -1 and 1. For chemotaxis in response to an attractant, as in this study, CI generally falls between 0 and 1; whereas in response to a repellent, CI usually falls between -1 and 0. CI=1 represents perfectly accurate chemotaxis in which cell displacement is parallel to the gradient direction, and CI=0 indicates that the cells' migration is unbiased. The facts that CI is bounded and dimensionless make it easy to compare different values across different experimental conditions and get an intuitive picture for the type of cell dynamics it represents.

We measure directional persistence using the chemotactic ratio (CR), defined as the ratio of the magnitude of the cell's displacement to the total distance traveled [59, 60, 87] (Figure 3.2),

$$CR \equiv \left\langle \frac{|\text{displacement}|}{\text{distance}} \right\rangle$$

CR is also dimensionless and bounded between 0 and 1, and once again intuitive sense can be made of either limit. If CR=1, then the cells are moving in perfectly straight lines. In contrast, CR=0 is representative of a cell trajectory that starts and ends near the same location on average.

We measure speed using the instantaneous speed along the trajectory. That is, we take the distance traveled in the measurement interval Δt (15 minutes in the experiments, see below), divide it by the interval, and average this quantity over all intervals that make up the trajectory.

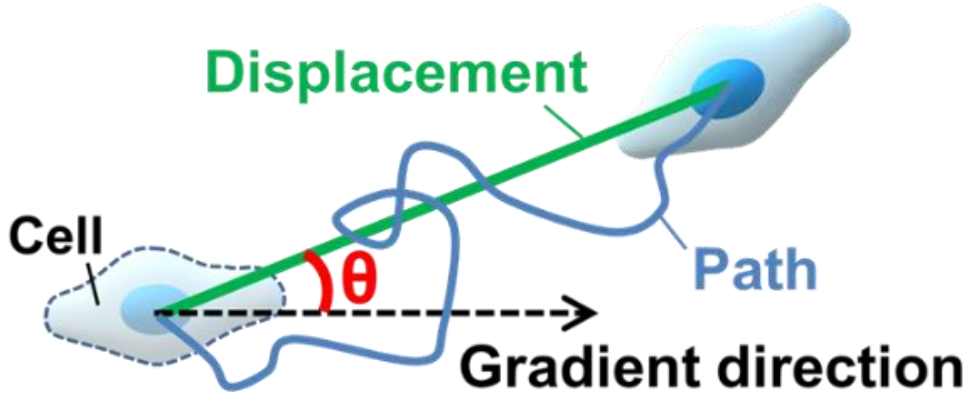

Figure 3.2. Illustration of characterization of the measured cell trajectory. The cell's displacement makes an angle θ with the gradient direction. The chemotactic index (CI) is defined here as the ratio of the displacement in the gradient direction to the total displacement. The chemotactic ratio (CR), also denoted as directional persistence (DP) is defined here as the ratio of the total displacement to the total distance traveled.

3.3.2 Breast cancer cells chemotax up TGF-β gradients

We begin by investigating the above properties of chemotaxis in the context of metastasis, specifically the epithelial-mesenchymal transition and subsequent invasion of cancer cells. To this end, we perform experiments using a triple-negative human breast cancer cell line (MDA-MB-231). Invasion of tumor cells *in vivo* is aided by external cues including soluble factors that are thought to form gradients in the tumor microenvironment [4, 9, 18, 26, 79, 80, 89]. Among these soluble factors, transforming growth factor-β (TGF-β) is a key environmental cue for the invasion process. Therefore, we use TGF-β as the chemoattractant [3, 4, 89-92].

The *in vivo* tumor microenvironment is highly complex. As a result, *in vivo* platforms have been developed and widely used to investigate the cancer response to a specific cue. In this study, a microfluidic platform is used to expose the TGF-β gradient to the cells in 3D culture condition (Figure 3.2 A). The microfluidic device is designed with three different channels, a center, source, and sink channel (Figure 3.2 B). The center channel is filled with a composition of MDA-MB-231 cells and type I collagen while the medium is perfused through the side source and sink channels. TGF- β is applied only through the source channel, not the sink channel, and therefore a graded profile develops over time in the center channel by diffusion. Consequently, the MDA-MB-231 cells surrounded by type I collagen are exposed to a chemical gradient of TGF- β.

To verify that a graded TGF- β profile is generated in the center channel, we utilize 10kDa FITC-dextran whose hydrodynamic radius (2.3nm) is similar to that of TGF- β (approximately 2.4 nm[93]). The fluorescence intensity is shown in Figure 3.2 C. The profile approaches steady state within 3 hours, is approximately linear, and remains roughly stationary for more than 12 hours. Therefore, we record the MDA-MB-231 cells using time-lapse microscopy every 15 minutes from 3 to 12 hours after imposing the TGF- β.

First, we perform a control experiment with no TGF- β to characterize the baseline of the MDA-MB-231 cell migratory behavior. Representative trajectories are shown in Figure 3.3 A, and we see that there is no apparent preferred direction. Indeed, as seen in Figure 3.3 C (black), the CI is centered around zero, indicating no directional bias. Notably, the spread of the CI values is very broad, with many data points falling near the endpoints -1 and. This is a generic feature of the CI due to its definition as a cosine: when the distribution of angles θ is uniform, the distribution of cosθ is skewed toward -1 and 1 because of the cosine's nonlinear shape. Nonetheless, we see that the median of the CI is very near zero as expected. The speed and CR are shown in Figure 3.3 D

and E, respectively (black). We see that the CR is significantly above zero, indicating that even in the absence of any chemoattractant, cells exhibit persistent motion. This result is consistent with previous works that showed that cells cultured in 3D tend to have directionally persistent movement unlike those in 2D [61].

Next, we expose cells to a TGF- β gradient of g = 50nM/mm. Representative trajectories are shown in Figure 3.3 B, and we see a possible bias in the gradient direction. Indeed, as seen in Figure 3.3 C (red), the CI is centered above zero, indicating a directional bias, and the difference with the control distribution is statistically significant ($p < 0.05$). We also see in Figure 3.3D (red) that the speed increases, although we will see below that the increase is relatively small and that the trend is not necessarily monotonic. Finally, we see in Figure 3.3 E (red) that the CR decreases, although the difference with the control is not statistically significant. These results suggest that a TGF-β gradient causes a significant increase in directional bias (CI) but not necessarily a significant change in cell speed or persistence (CR).

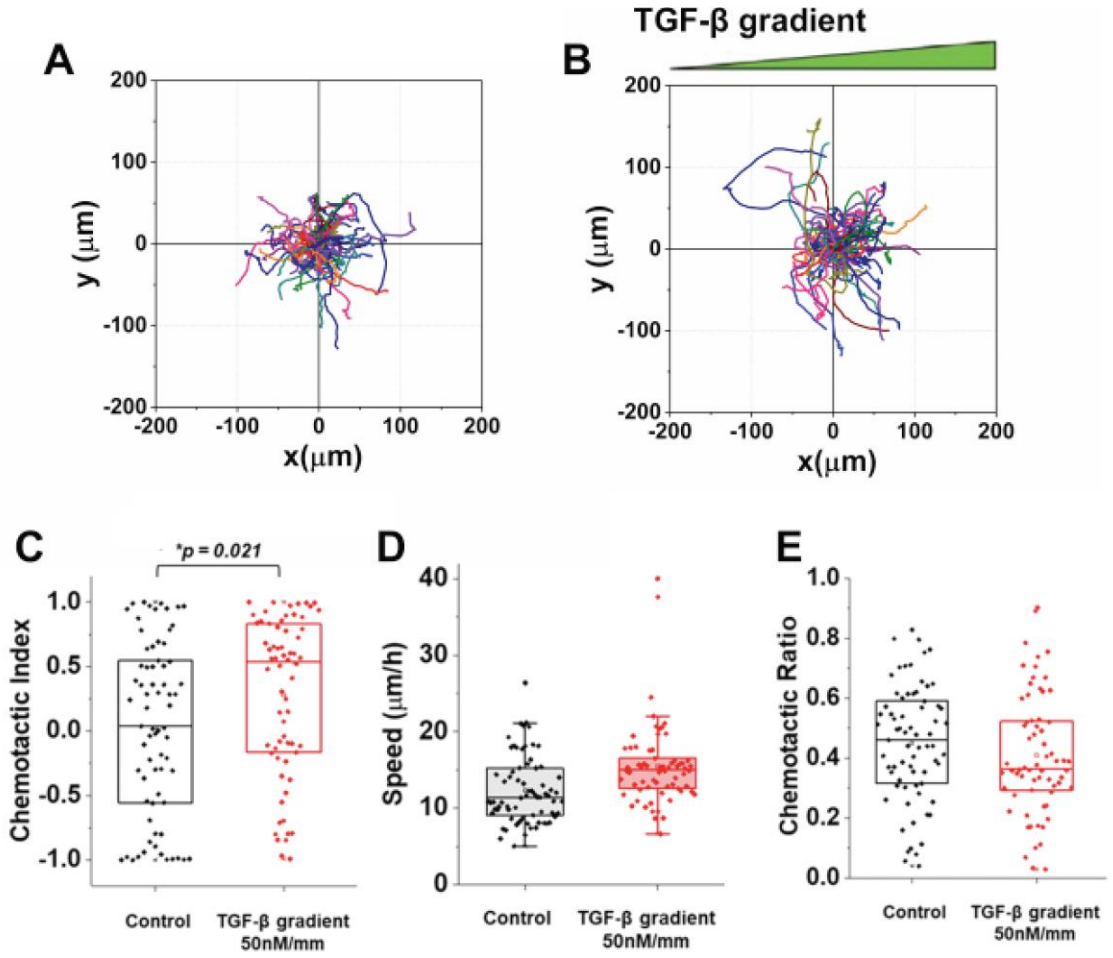

Figure 3.3. Cell trajectories and chemotactic performance in TGF-β gradient. Cell trajectories of (A) control and (B) 50nM/mm TGF-β gradient. Distribution of (C) chemotactic index, (D) speed, (E) chemotactic ratio of each trajectory from both the control (black) and the TGF-β gradient (red). Boundary of box plots indicates quadrants with centerline as median. Distributions are statistically compared using Mann-Whitney test.

To confirm the trends suggested above, we evaluate the response to four different TGF- β gradient strengths, g= 0, 1, 5, and 50nM/mm, in three separate experiments each (Figure 3.4 A-C). We see in Figure 3.4 A that, consistent with Figure 3.3, the CI is zero for the control and increases with gradient strength g. In fact, the CI appears to saturate beyond 5nM/mm, such that its value at 50nM/mm is not significantly larger than its value at 5nM/mm. We also see in Figure 3.4 B, consistent with Figure 3.3, the CR slightly decreases with the gradient strength although the decrease is roughly within error bars. Finally, we see in Figure 3.4C that the increase in the speed is small, achieving a statistically significant difference with the control only at the largest gradient strength, and that the trend is not monotonic.

3.3.3 Minimum detectable gradient is shallow

A striking feature of Figure 3.4 A is that the cells respond to a gradient as shallow as g = 5nM/mm. To put this value in perspective, we estimate both the relative concentration change and the absolute molecule number difference across the cell body [33]. The microfluidic device is about 1mm in the gradient direction, and therefore a cell in the middle experiences a background concentration of about c = 2.5nM. Assuming the cell is on the order of a = 10μm wide, the change in concentration across its body is ga= 0.05nM, for a relative change of ga/c = 2%. The number of attractant molecules that would occupy half the cell body is on the order of ca^3 = 1500. Two percent of this is ga^4 = 30, meaning that cells experience about a thirty-molecule difference between their two halves. The same quantities are approximately ga/c = 1% and 6%, and ga^4 = 60 and 300, for amoebae in cyclic adenosine monophosphate gradients [44] and epithelial cells in epidermal growth factor gradients[25], respectively [33]. This suggests that the response of MDA-MB-231 cells to TGF-β gradients is close to the physical detection limit for single cells.

3.3.4 Cellular potts model simulation

To understand the experimental observation that the CI increases with gradient strength, but the CR and speed do not (Figure 3.4), the experimental results are compared with computational model. [94] We use a 2D simulation of chemotaxis of a cell through an extracellular medium, namely the cellular Potts model (CPM) [95, 96]. The reason that we use a 2D simulation is that, although cells are executing 3D migration through the collagen matrix, the microfluidic device is quasi-2D: its height is less than 100μm, whereas its width in the gradient direction is about 1 mm, and its length is several millimeters. Moreover, from the experimental trajectories (Figure 3.3) we have estimated that if motility fluctuations in the height direction are equivalent to those in the length direction, then the error in the CI that we make by the fact that we only observe a 2D projection of cell motion is less than 1%.

The CPM is a lattice-based simulation that has been widely used to model cell migration [97, 98]. In the CPM, a cell is defined as a finite set of simply connected sites on a regular square lattice. The cell adheres to the surrounding collagen with an adhesion energy α and has a basal area A_0 from which it can fluctuate at an energetic cost λ. This gives the energy function

$$u = \alpha P + \lambda (A - A_0)^2$$

where P and A are the cell's perimeter and area, respectively.

Cell motion is a consequence of minimizing the energy *u* subject to thermal noise and a bias term *w* that incorporates the response to the gradient [97]. Specifically, for a lattice with L total sites, one update step occurs in a fixed time τ and consists of L^2 attempts to copy a random site's label (cell or non-cell) to a randomly chosen neighboring site. Each attempt is accepted with probability

$$\mathrm{P} = \begin{cases} e^{-(\Delta u - w)} & \Delta u - w > 0 \\ 1 & \Delta u - w \le 0 \end{cases}$$

where Δu is the change in energy associated with the attempt. The bias term is defined as

$$w = \Delta x \cdot \vec{p}$$

where Δx is the change in the cell's center of mass caused by the attempt, and $\vec{p}$ is the cell's polarization vector, described below. The dot product acts to bias cell motion because movement parallel to the polarization vector results in a more positive w, and thus a higher acceptance probability.

The polarization vector is updated every time step τ according to

$$\frac{\Delta \vec{p}}{\tau} = r\left(-\vec{p} + \eta \Delta \hat{x}_{\tau} + \delta \vec{q}\right)$$

The first term in the above equation represents exponential decay of $\vec{p}$ at a rate *r*. Thus, r^{-1} characterizes the polarization vector's memory timescale. The second term causes alignment of $\vec{p}$ with $\Delta \hat{x}_{\tau}$ according to a strength η, where $\Delta \hat{x}_{\tau}$ is a unit vector pointing in the direction of the displacement of the center of mass in the previous time step tau. Thus, this term promotes persistence because it aligns $\vec{p}$ in the cell's previous direction of motion. The third term causes alignment of $\vec{p}$ with $\vec{q}$ according to a strength ε, where $\vec{q}$ contains the gradient sensing information, as defined below. Thus, this term promotes bias of motion in the gradient direction.

The sensing vector $\vec{q}$ is an abstract representation of the cell's internal gradient sensing network and is defined as

$$\vec{q} = \left\langle (n_i - \bar{n}) \hat{r}_i \right\rangle$$

where the average is taken over all lattice sites i that comprise the cell. The unit vector $\hat{r}_i$ points from the cell's center of mass to site *i*, the integer n_i represents the number of TGF-β molecules detected by receptors at site *i*, and $\bar{n}$ is the average of n_i over all sites. The integer n_i is the minimum of two quantities: (i) the number of TGF-β receptors at site *i*, which is sampled from a Poisson distribution whose mean is the total receptor number N divided by the number of sites; and (ii) the number of TGF-β molecules in the vicinity of site *i*, which is sampled from a Poisson distribution whose mean is $(c + gx_i)\ell^3$, where ℓ is the lattice spacing, and x_i is the position of site *i* along the gradient direction. Taking the minimum incorporates receptor saturation, since each site cannot detect more attractant molecules than its number of receptors. The subtraction in the equation of $\vec{q}$ makes $\vec{q}$ a representation of adaptive gradient sensing: if receptors on one side of the cell detect molecule numbers that are higher than those on the other side, then $\vec{q}$ will point in that direction.

The simulation is performed at a fixed background concentration *c* and gradient *g* for a total time *T*. The position of the cell's center of mass is recorded at time intervals Δt, from which we compute the CI, CR, and speed.

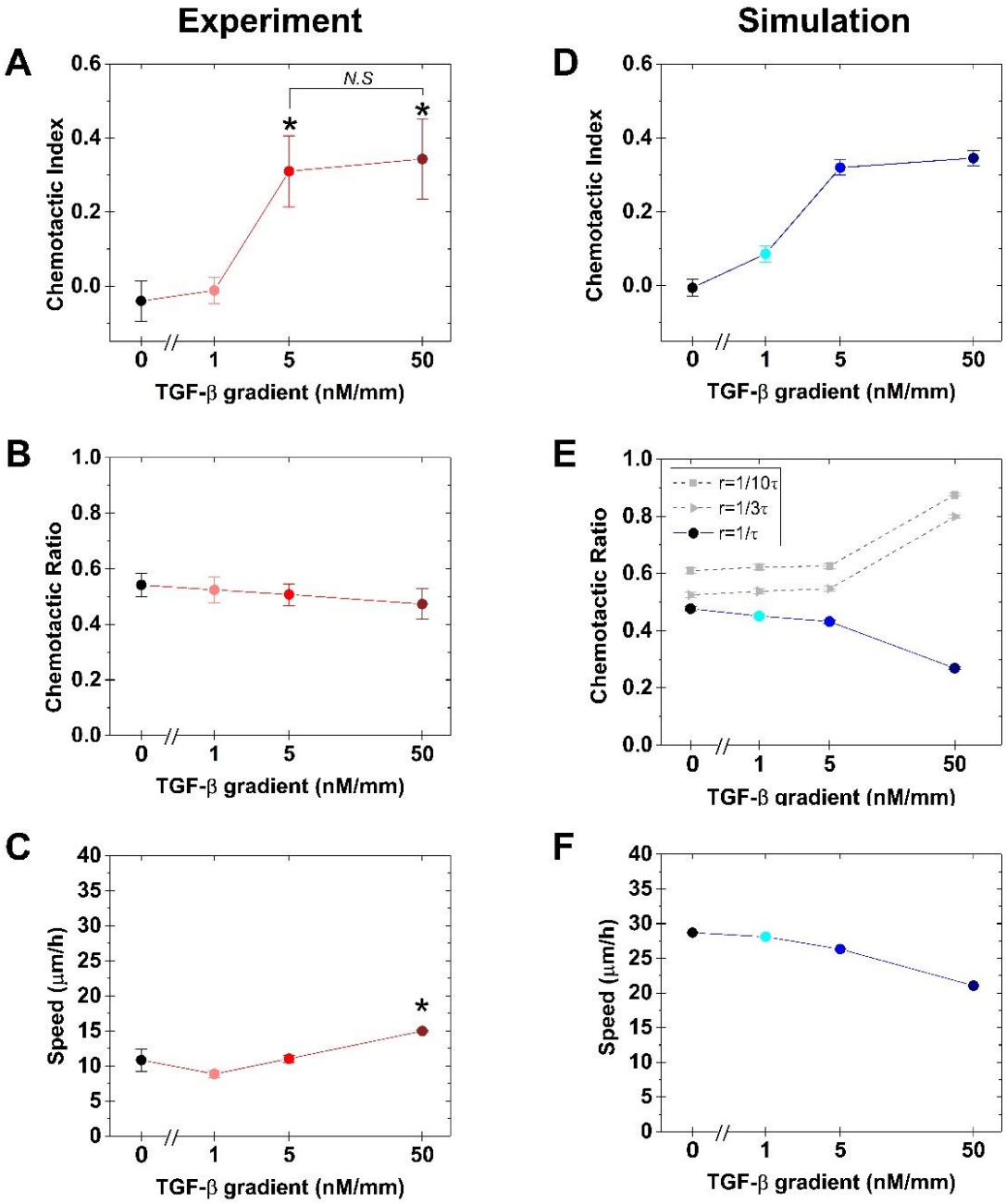

Figure 3.4. Chemotactic performance for different strength of TGF-β gradients. Experimental (A) chemotactic index, (B) chemotactic ratio, and (C) speed for four different TGF-β gradients g=0, 1, 5, and 50nM/mm. (red) Data points indicate average and standard error of medians from three different experiments. A, B, and C are plotted with log-scaled TGF-β gradient. (D-f) same for cellular Potts model (CPM) simulation (blue). Error bars are standard error from 1000 trials.

3.3.5 Theoretical model reveals performance constraints

Our finding that bias and persistence are decoupled in the simulations allow us to appeal to a much more simplified theoretical model in order to understand and predict global constraints on chemotaxis performance. Specifically, we consider the biased persistence random walk (BPRW) model [99, 100], in which bias and persistence enter as explicitly independent terms controlled by separate parameters. The BPRW has been shown to be sufficient to capture random and directional, but not periodic, behaviors of 3D cell migration [101]. Because we do not observe periodic back- and forth motion of cells in our experiments, we propose that the BPRW is sufficient to investigate chemotactic constraints here.

As in the simulations, we consider the BPRW model in 2D. In the BPRW model, a cell is idealized as a single point. Its trajectory consists of M steps whose lengths are drawn from an exponential distribution. We take $M = T/\Delta t = 36$ as in the experiments. The probability of a step making an angle θ with respect to the gradient direction is

$$P(\theta \mid \theta') = \underbrace{b\cos\theta}_{\text{bias}} + \underbrace{\frac{e^{p\cos(\theta-\theta')}}{2\pi I_0(p)}}_{\text{persistence}}$$

where θ' is the angle corresponding to the previous step. The first term incorporates the bias, with strength b. It is maximal when the step points in the gradient direction ($\theta = 0$) and therefore promotes bias in that direction. It integrates to zero over its range ($-\pi < \theta < \pi$) because the bias term only reshapes the distribution without adding or subtracting net probability. The second term incorporates the persistence, with strength p. It is a von Mises distribution (similar to a Gaussian distribution, but normalized over the finite range $-\pi < \theta < \pi$) whose sharpness grows with p. It is maximal at the previous angle θ' and therefore promotes persistence. The normalization factor I_0 is the zeroth-order modified Bessel function of the first kind.

The requirement that $P(\theta|\theta')$ be non-negative over the entire range of θ mutually constrains b and p. However, apart from this constraint, b and p can take any positive value. We sample many pairs of b and p, reject those that violate the constraint, and compute the CI and CR from a trajectory generated by each remaining pair. The results are shown in Figure 3.5 (colored circles). We see in Figure 3.5 that the BPRW model exists in a highly restricted 'crescent' shape within CI-CR space. As expected, the CI increases with the bias parameter b (color of circles, from blue to

red). The top corner corresponds to maximal bias and no persistence; indeed, when $p=0$ the persistence term reduces to $(2\pi)^{-1}$ and non-negativity requires $b<(2\pi)^{-1} \approx 0.16$, which is consistent with the upper limit of the color bar. Also, as expected, the CR increases with the persistence parameter p (size of circles, from small to large), although only in the lower portion where the CI is low.

The crescent shape implies that several modes of chemotaxis are prohibited under our simple model. For example, it is not possible to have high bias without any persistence (CI → 1, CR → 0). It is also not possible to have high persistence with intermediate bias (CR →1, CI → 0.5). Finally, we see that as the CI increases, the range of allowed CR values becomes progressively more restricted.

The crescent shape can also be compared with the data from the simulations and experiments, which are overlaid in the blue and red squares in Figure 3.5, respectively. The shape of the crescent is such that if a cell has a low CI but a high CR (bottom right corner of the crescent) and its CI increases, its CR must decrease. This restriction helps explain why, in the simulations and experiments, as the CI increases, we do not see the CR also increase, but instead we see the CR decrease (Figure 3.5, squares). A simultaneous increase in CI and CR from this starting position is simply not possible according to the model. This simple feature of the BPRW is sufficient to explain the way in which accuracy and persistence are mutually constrained during the chemotaxis response of these cells.

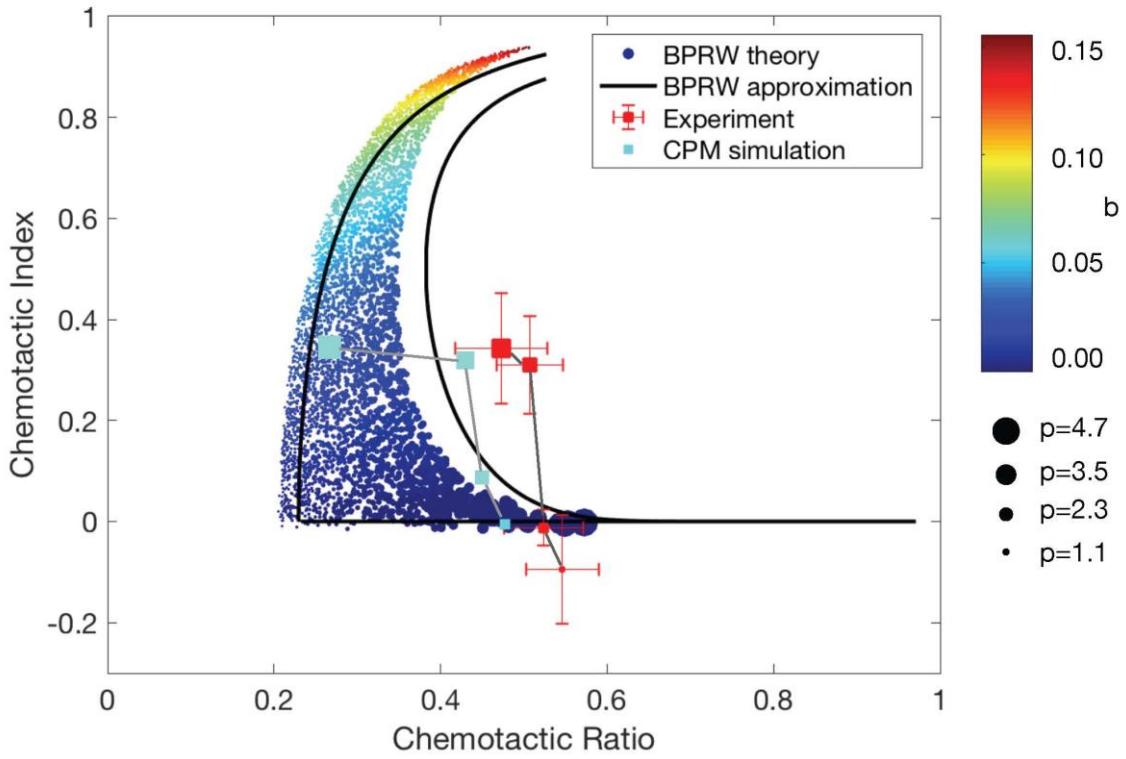

Figure 3.5. Comparison of theory with experiments and simulations.

3.4 Discussion

By integrating experiments with theory and simulations, we have investigated mutual constraints on the accuracy (CI), persistence (CR), and speed of cell motion in response to a chemical attractant. We have found that while the CI of breast cancer cells increases with the strength of a TGF-β gradient, the speed does not show a strong trend, and the CR slightly decreases. The simulations suggest that the decrease in CR is due to a decoupling between sensing and persistence in the migration dynamics. The theory confirms that the decrease in CR is due to a mutual constraint on accuracy and persistence for this type of decoupled dynamics, and more generally, it suggests that entire regions of the accuracy-persistence space are prohibited.

Several predictions arise from our work that would be interesting to test in future experiments. First, our simulation scheme assumes that the saturation of the CI with gradient strength is due to limited receptor numbers. However, alternative explanations exist that are independent of the receptors, such as the fact that it is more difficult to detect a concentration

difference on top of a large concentration background than on top of a small concentration background due to intrinsic fluctuations in molecule number [25, 102]. An interesting consequence of our mechanism of receptor saturation is that, at very large gradients (beyond those of Figure 3.4). the CI would actually decrease because all receptors would be bound. It would be interesting to test this prediction in future experiments.

Second, our work suggests that not all quadrants of the accuracy-persistence plane are possible for cells to achieve (Fig 9). It would be interesting to measure the CI and CR of other cell types, in other chemical or mechanical environments, to see if the crescent shape seen in Fig 9 is a universal restriction, or if not, what new features of chemotaxis are therefore not captured by the modeling. In this respect, the work here can be seen as a null model, deviations from which would indicate new and unique types of cell motion.

4. CELLULAR SIGNAL PROCESSING CAPACITY CONSTRAINTS CANCER CELL CHEMOTAXIS UNDER MULTIPLE CUES

4.1 Introduction

Chemotaxis is a systematic cellular response requiring signal sensing, cell polarization, and cell motility. Signaling networks are critical to the chemotactic response of cells. In regulating the cellular responses, some signaling pathways, such as G-protein mediated pathways, are activated through receptors for either growth factors or chemokines[10, 103]. It has been demonstrated that chemotaxis is triggered by binding the growth factors/chemokines to corresponding receptors, including G-protein coupled receptors (GPCR) and receptor tyrosine kinases (RTK) [4]. The small GTPases within the Rho subfamily have been known to regulate actin polymerization, microtubule dynamics, and directional sensing, which play critical roles in chemotaxis [103-105].Crosstalk between either receptors or pathways can adjust the downstream function of the pathways [106-108]. Indeed, the EGFR cascade, which is an example of RTK, cross-communicates with the GPCR-mediated chemotaxis pathways in breast cancer [106]. Also, EGFR signaling can be induced by CXCR4 activation binding with stromal cell-derived factor-1α (SDF-1α), resulting in cooperative function in cell metastasis [107]. RTKs are also known to interplay with transforming growth factor-β (TGF-β) through Smad-dependent transcription or PI3K/AKT activation [108].

Many different types of cancer cells are known to chemotax towards single chemical cues [4, 94, 109-112]. Metastatic breast cancer cells surrounded by collagen matrix migrate in response to a TGF-β gradient [94]. An EGF gradient also induces chemotaxis in breast cancer cells [109, 110]. An SDF-1α gradient induces biased migration in various types of cancer, including breast [111] and pancreatic [112] cancer cells. In addition to a single cue, the combined effect of two growth factors has also been investigated considering the signaling crosstalk between the cues [30, 113-115] . A cooperative effect of EGF and SDF-1α gradients mediating breast cancer chemotaxis was reported by Mosadegh et al [113]. In addition, Uttamsingh et al [30] showed a synergistic effect of EGF and TGF-β in inducing invasion/migration capability in epithelial cells. When the rat intestine epithelial cells were simulated by both growth factors, the invasion/migration of cells in Boyden chamber were highly enhanced. Effect of TGF-β inducing epithelial-mesenchymal transition was considered to cooperate the CCL7-mediated chemotaxis [115]. The combined effect of TGF-β, EGFR, and HER2 pathways was implemented to developing targeted therapy for

pancreatic adenocarcinoma [114]. By targeting TGF-β pathways combined with EGFR and HER2, the capability of lymphatic metastasis was highly suppressed.

Despite the research advances in acknowledging cross actions of multiple signals, how cells are sensing and deciphering complex chemical cues is still poorly understood. In the TME, cells are exposed to chemical cues whose chemical composition is complex, and the physical nature is also complex. Research efforts have been focused on the chemical composition and associated downstream signaling pathways. However, signaling pathway is highly complex even for a single receptor activation. The intracellular signaling networks involve a series of intracellular processes relevant to diverse cell physiological responses, not specific. [90, 116]. The complexity in the signaling networks has been an extreme barrier to predict and illustrate the cellular response, specifically for chemotaxis induced by multiple cues. The effects of physical nature of multiple chemical cues and associated cellular signal transduction performance are not well studied on cellular migratory behavior. We still do not understand how cells integrate signals from multiple chemical cues in their migratory behavior.

In this study, we investigate how cells process and decipher multiple chemical cues with various physical natures. We hypothesize that cancer cell chemotaxis is regulated not only by the biochemical nature of signals, but also by physical characteristics including signal strength, signal-to-noise ratio, and background levels of the chemical cues. We test this hypothesis by experimental and theoretical analysis of cancer cell chemotaxis in response to TGF-β and EGF cues. These two chemical cues are selected since these have been reported to promote chemotaxis of cancer cells [94, 110] and the effects of combined cues are anticipated to be synergistic or at least additive [30]. Experimentally, migratory behaviors of cancer cells within a 3D matrix are assessed in response to single and multiple cues of TGF-β1 (denoted as TGF-β) and EGF by use of a microfluidic platform. On the microfluidic platform, chemical cues of TGF-β and EGF are created with different gradient strengths, and background concentrations. Contrary to our initial anticipation, we observe significant antagonism of chemotactic behaviors which cannot be explained with a crosstalk with TGF-β and EGF signaling pathways. To explain this counter intuitive result, we develop a novel biophysical framework that can explain different types of chemotactic response in multiple cue cell migration experiments and propose quantitatively testable predictions. The predictions with controllable background noise levels of the growth factors are then validated by the experiment.

4.2 Materials and methods

4.2.1 Cell culture and reagents

Human breast adenocarcinoma cells (MDA-MB-231) were cultured in Dulbecco's Modified Eagle Medium/Ham's F-12 (Advanced DMEM/F-12, Lifetechnologies, CA, USA) supplemented by 5% v/v fetal bovin serum (FBS), 2 mM L-glutamine (L-glu), and 100 μg ml^{-1} penicillin/streptomycin(P/S) for less than 15 passages. MDA-MB-231 cells were regularly harvested by 0.05% trypsin and 0.53mM EDTA (Lifetechnologies,CA, USA) when grown up to around 80% confluency in 75 cm^2 T-flasks at 37°C with 5% CO_2 incubation. Harvested cells were used for experiments or sub-cultured. Murine pancreatic cancer cell line, eKIC isolated from genetically engineered mouse model (GEM) of PDAC. The KIC cells were established form KIC mice in which *Kras* was combined with deletion of the *Ink4a* locus (*Ink4a/Arf*$^{L/L}$) to generate the *Pdx1-Cre;LSL-Kras*^{G12D}*;Ink4a/Arf*$^{-/-}$ GEM. [117, 118] These cells were maintained in RPMI 1640 with 2.05mM L-glutamine (GE Healthcare Bio-Sciences Corp., MA, USA) supplemented by 5% v/v fetal bovine serum (FBS) and 100 μg ml^{-1} penicillin/streptomycin (P/S). The cells were regularly harvested by 0.05% trypsin and 0.53mM EDTA (Life technologies, CA, USA) when grown to ~80% confluency in 75 cm^2 T-flasks and incubated at 37°C with 5% CO_2. Harvested cells were used for experiments, or sub-cultured while maintaining them below 15th passage.

4.2.2 Chemotaxis assay

For the chemotaxis assay, cells were implanted in the chemotaxis platform, which is an *in vitro* microfluidic device developed to engineer the chemical environment. To investigate the cellular response to the gradient signals by observing the cell migratory behaviors, we use an engineered chemotaxis platform developed in a microfluidic device, as shown in **Fig. S1**. The chemotaxis platform was designed for engineering the chemical environment surrounding the cells embedded in the 3D extracellular matrix. The platform is composed of three microfluidic channels with 100μm in thickness. A center channel of 1mm wide, which aims to contain cells with a collagen matrix, is located in between source (top) and sink (bottom) channels with 300μm wide. At the end ports, the source and sink channels are connected to large reservoirs so that the culture medium can be supplemented through the channels. For the cell culture, the basic culture medium is filled in both source and sink channels. In order to develop a concentration gradient in the center channel, growth factor solution (TGF-β or EGF) based on the medium is added through the source

channel. On the other hand, the sink channel is filled with growth factor-free medium. Assuming that there is neither flow nor any pressure differences between the channels, the concentration of the given growth factor (*i*) can be illustrated by the conservation equation of chemical species:

$$\frac{\partial C_i}{\partial t} = D_i \cdot \nabla C_i \tag{1}$$

At the steady state, the concentration profile in the center channel goes to a linear. The linear profile can persist for a while with an assumption that is the concentration at the source and side channels are constant with a large volume of reservoirs. Consequently, cells cultured in the collagen matrix are exposed to a linear gradient of a specific soluble factor. The detailed technique to develop the microfluidic device and the diffusion principle in the platform was described in prior chapter 3 [94].

Cells were embedded uniformly to type I collagen mixture (Corning Inc., NY, USA) supplemented with 10X PBS, NaOH, HEPE solution, FBS, Glu, P/S, and cell-culture level distilled water. Initial cell density was consistently 5×10^5 cells/ml for MDA-MB-231 and 8×10^5 cells/ml for eKIC respectively in the 2mg/ml type I collagen mixture. After loading, the cells in the collagen matrix were cultured with basic mediums for 24 hours. MDA-MB-231 cells were then exposed by serum-reduced medium for another 24 hours. The serum-reduced medium was supplemented by 1% v/v FBS instead of 5% v/v FBS in the basic medium. Due to a critical viability change in the serum-reduced culture condition (data is not shown), serum starvation was not conducted for eKIC. Then, cells were exposed by concentration gradients of growth factors, either Transforming growth factor beta-1 (TGF-β1, Invitrogen, CA, USA) or epidermal growth factor (EGF, Invitrogen, CA, USA).

4.2.3 Characterization of cell migration

Live-cell imaging technique with time-lapse microscopy was used to characterize cell migration. An inverted microscope (Olympus IX71, Japan) was equipped with a stage top incubator as described in [94], which allowed maintaining the microfluidic chemotaxis platform at 37ºC with 5% CO_2 environment during imaging. MDA-MB-231 cells in the chemotaxis platform were captured every 15 minutes for 9 hours. eKIC cells were captured every 5 minutes for 3 hours. The temporal intervals and durations for the time-lapse imaging were optimized for

each cell line by considering the cell motility, ~12μm/h for MDA-MB-231 and ~50μm/h for eKIC, respectively (Figure 4.3). In both cases, the time-lapse imaging was started 3 hours after applying the growth factors for sufficient adjusting time to develop gradient profiles accordingly. The bright-field images were further processed to analyze cell migration. The cell area was defined by using the contrast differences between cells and background and converted to monochrome images by using ImageJ. A cell trajectory was illustrated as a collection of the centroid positions of cell areas at different time points. In tracking the cell movement, we excluded the cells undergoing division to avoid extra effect for cell polarity [119]. Also, we excluded the stationary cells defined when the cells moved less than their diameter.

Biased cell motion is commonly characterized by directional accuracy, persistence, and motility [94]. We measure directional accuracy using the chemotactic index (CI)

$$CI = \cos\theta \tag{2}$$

where θ is the angle between the net displacement of a trajectory and the gradient direction. The displacement is defined as a straight line connecting the initial and final points of a trajectory where we measure each trajectory for 9 hours (**Figure. 3.2**). The CI can range between -1 and 1. Higher CI indicates more accurate chemotaxis in response to an attractant. CI = 1 means that the cell perfectly follows the gradient direction, whereas CI = 0 means that the cell is unbiased. Cells moving towards the opposite direction to the gradient have a negative CI between -1 and 0. In an experimental trial, multiple CIs are distributed throughout the range of -1 to 1 due to variations of cell response to the attractant. While each CI represents the directional accuracy of a single trajectory, we measure a median CI as a representative CI in a trial. Our previous study has shown that the CI distribution is U-shaped without any attractant, indicating that the cell migration directions are uniformly distributed; in contrast, the CI distribution with an attractant shows a biased distribution toward 1 [94]. In addition, motility is quantified as an instantaneous speed along the cell trajectory:

$$\text{Cell speed} = \frac{\textit{Path} \text{ of a trajectory}}{\textit{Duration}} \tag{3}$$

where the cell path is taken from a trajectory where measurement is taken every Δt = 15 minutes. In our previous study for the physical constraints of the breast cancer chemotaxis [94], we have shown that the directional accuracy is a dominant metric in the chemotaxis of the 3D cultured cells migrating in ECM whereas cell persistence is barely changed by the chemical gradient. In this study, we mainly discuss the chemotaxis with the accuracy and motility, excluding the persistence.

4.2.4 Statistical analysis

In evaluating the chemotactic characteristics, more than 30 trajectories were analyzed in an experimental trial, which was repeated at least three times for all experimental groups. Each trajectory was quantified as CI and speed. To evaluate the chemotactic accuracy, medians of CIs from the repetitions were averaged and reported in a bar (Figure 4.2B, 4.5B, and 4.6A) with an error bar representing a standard estimated error (S.E.). For the simulation, CIs were collected from 400 cell trajectories in a control group and reported as an average ± S.E. of the CIs of 400 trajectories. Differences in CIs presented in the bar graphs were statistically analyzed by student t-test. The significant changes between comparisons were examined when the p value < 0.05. In addition, all collected CIs and speeds in a group were reported in box plots. A data point in the box plots in Figure 4.2-4.6 indicates each metric of a cell trajectory showing the distribution characteristics of the metric in a group. For the speeds in Figure 4.3, Tukey's *post hoc* test in ANOVA was used to assess the statistical significance when the p value < 0.05.

4.3 Results

4.3.1 Chemotaxis in breast cancer cells is induced by a gradient of TGF-β or EGF

Diverse soluble factors, including TGF-β and EGF, guide biased cell motion *in vivo* in concentration gradient forms [4, 10, 34] . In sensing the gradient, cells can detect the concentration differences through ligand-receptor activations at different cell surface locations, as illustrated in Figure 4.1A. Sensing the gradient results in the biased movement of the cells. First, we investigate the chemotactic response of the cells to a single cue. In this study, we use a triple-negative breast cancer cell line MDA-MB-231, which has been recognized as a highly metastatic cell type [120] . Chemotactic response of MDA-MB-231 has been reported with several growth factors, including

TGF-β and EGF [94, 109]. Here, we investigate the effect of a gradient of either TGF-β or EGF in the chemotaxis platform to confirm the chemotactic response of cells. A linear gradient of the soluble factor is exposed to cells surrounded by type I collagen matrix as described in 4.2 m**aterials and methods section**. By measuring the cell trajectories (Figure 4.1B), we quantify the chemotactic behaviors of cells with chemotactic index (CI) indicating the directional accuracy which is expressed as the ratio of the displacement of a cell trajectory in the gradient direction to the total displacement of the cell trajectory. Consistent with the results of breast cancer cell migration in response to a TGF-β gradient of 50 nM/mm from our previous work [94], we see an apparent bias in cell migration when cells are moving in response to a TGF-β gradient (Figure 4.2 A). The cell response to an EGF gradient of 800 nM/mm is also biased as shown in Figure 4.2 A and Figure 4.4. The statistics from all trials are shown in Figure 4.2B and C, and we see that whereas in the control case the CI distribution is U-shaped with a median near zero (gray), in the TGF-β (red) and EGF (blue) cases the CI distributions are highly biased toward 1 with positive median values, indicating that cells follow the gradient. These results confirm that, in addition to TGF- β, the EGF gradient is also capable of guiding biased cancer cell migration by promoting directional accuracy. Both TGF-β and EGF promote cell motility without any significant difference between the two cases (**Fig. S3**), verifying the effect of TGF-β and EGF in promoting intrinsic cell motility.

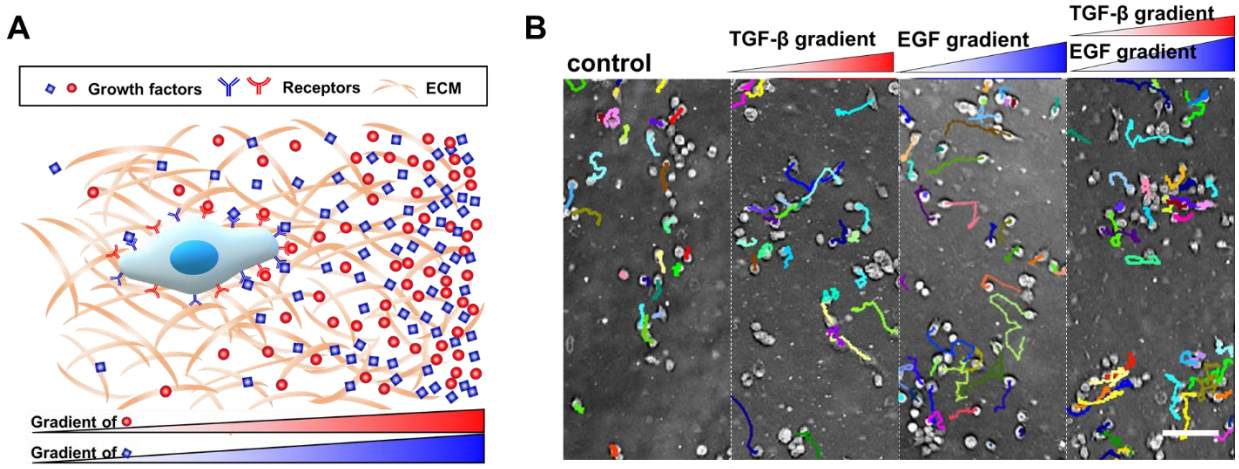

Figure 4.1. Illustration of chemotaxis and chemotaxis measurement. (A) Schematic description of cell chemotaxis in the tumor microenvironment (TME). (B) Micrograph of MDA-MB-231 cells in the chemotaxis platform at the end time of the trajectory measurement.

4.3.2 Breast cancer cells show an antagonistic response to combined TGF- β and EGF gradients

To understand the effect of the complex tumor microenvironment containing various soluble factors, we investigate the cellular migratory response to combined chemical cues. TGF-β and EGF bind to independent receptors on the MDA-MB-231 cell surface. To elucidate the effect of combined signals on chemotaxis, we expose both TGF-β and EGF gradients simultaneously to the cells by using the chemotaxis platform. Surprisingly, the chemotactic index in response to the combined gradients decreases compared to each individual gradient case (Figure 4.2 B), which we call ‘antagonism’. The distribution of CI values is also less biased than the single gradient cases (Figure 4.2 C). It is a remarkable result since many studies have reported the functional cooperation of multiple signals rather than the antagonism that we see here [30, 115]. It might be possible that although breast cancer cells do not share the same receptors for sensing TGF-β and EGF gradients, there might be a convergent downstream in the signaling pathway that governs biased migration, common to both cues.

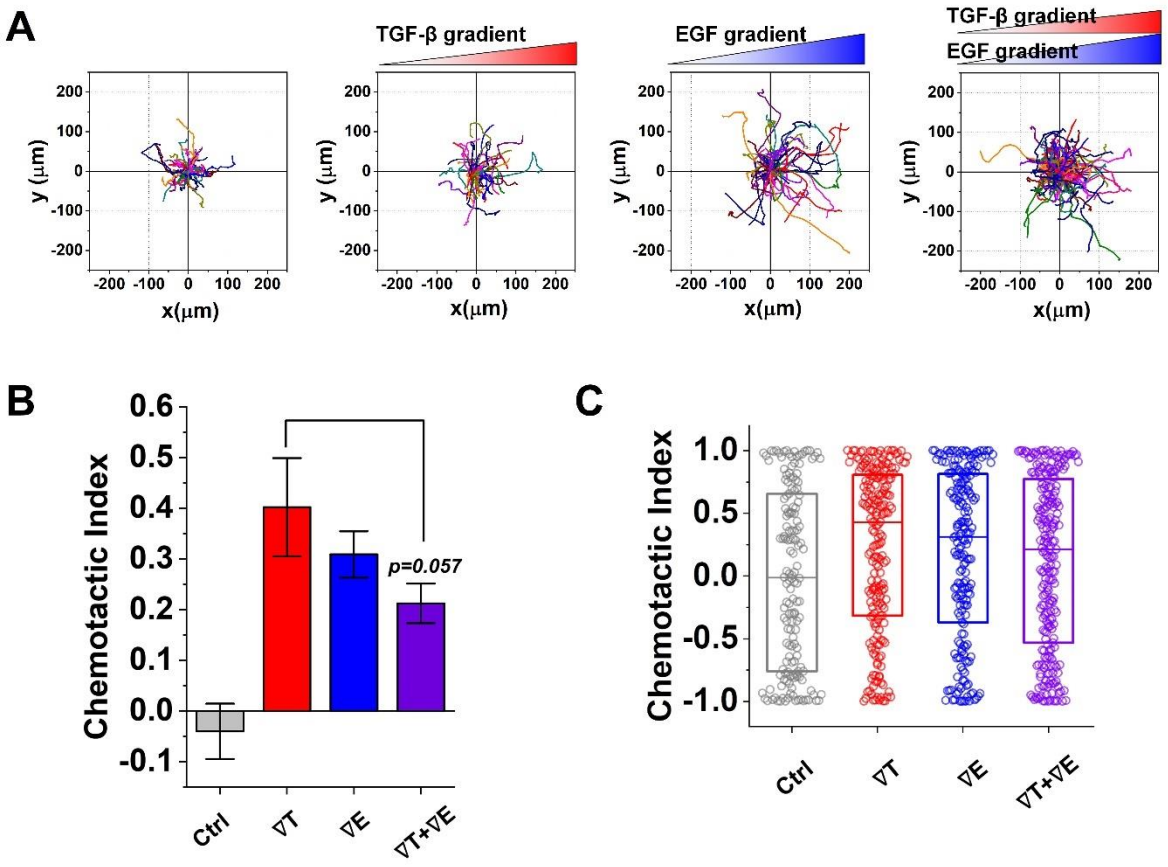

Figure 4.2. Breast cancer cells chemotax up individual TGF-β and EGF gradients more strongly than when gradients are combined (antagonism). Cell trajectories of (A) control, 50nM/mm TGF-β gradient (∇T), 800nM/mm EGF gradient (∇E), and combined gradients of 50nM/mm TGF-β with 800nM/mm EGF (∇T+∇E). (B) Averages of medians of chemotactic index (CI). n≥3. Bar: mean ± S.E. (C) CI distribution of all trajectories. Dot: CI from a single trajectory. Box: quartiles with a median line in the middle of the box.

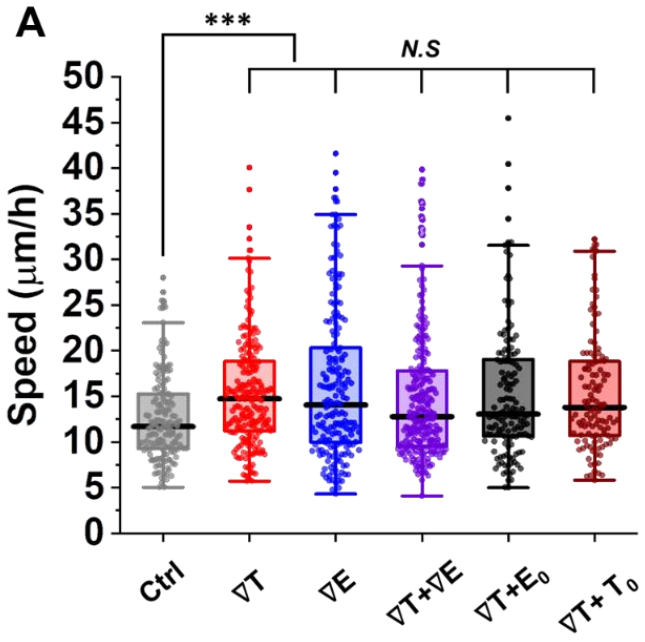

Figure 4.3. Speed distribution of collected trajectories from all experimental groups. Control (ctrl), 50nM/mm TGF-β gradient (∇T), 800nM/mm EGF gradient (∇E), combined gradients of 50nM/mm TGF-β with 800nM/mm EGF (∇T+∇E)**,** combination of 50nM/mm TGF-β gradient with 400nM EGF background (∇T+E_0), and combination of 50nM/mm TGF-β gradient with 25nM TGF-β background (∇T+T_0) of MDA-MB-231; Dot; speed from a single trajectory. Box: interquartile range (IQR) ± 1.5 IQR whiskers with a mean line in the middle of the box. *: p<.05, ***: p<.001 (ANOVA Tukey's *post hoc* test).

4.3.3 Mathematical model predicts the presence of a common saturating component responsible for antagonism

To understand the antagonism observed in the experiments, a simple model is proposed to describe biased cell migration in response to chemical gradients. The most natural hypothesis for a reaction pathway that can lead to antagonism is mutual repression: TGF-β would activate migration through pathway one, and EGF through pathway two, but TGF-β would also repress pathway two and vice versa. However, we are not aware of experimental evidence for such repressive crosstalk between the TGF-β and EGF pathways in breast cancer cells. Here, we suggest a simpler alternative that is based on the saturation of a common pathway component. We suppose that there is a molecular species M common to both the EGF and TGF-β pathways that drive the cell migratory response. M is converted to an active form M* by either EGF (E) or TGF-β (T), and M* then propagates the signal further downstream in the pathway (Figure 4.4 A). In our model, M is converted to M* with rate k_T by TGF-β and with rate k_E by EGF, and M* is converted to M with a rate of 1 which sets the timescale for the system.

$$\mathrm{T}+\mathrm{M} \xrightarrow{k_T} \mathrm{T}+\mathrm{M}^* \tag{4}$$

$$\mathrm{E}+\mathrm{M} \xrightarrow{k_E} \mathrm{E}+\mathrm{M}^* \tag{5}$$

$$\mathrm{M}^* \xrightarrow{1} \mathrm{M} \tag{6}$$

A TGF-β or EGF gradient is translated into a difference in M* molecules between the forward and backward halves of the cell (Figure 4.4A). We therefore take the difference ΔM^* to be the output of the model. The statistics of ΔM^* can be found by recognizing that conversion to M^* or vice versa is a binomial process (Supplementary information). In steady state, the signal to noise ratio (SNR) is given by,

$$SNR = \frac{\overline{\Delta M^*}}{\sigma_{M^*}} = \frac{\grave{\mathrm{O}}}{1+\eta+\beta}\sqrt{\frac{M_0\beta(1+\eta)}{2}} \tag{7}$$

where the dimensionless parameters η, β, and ϵ are defined as,

$$\eta = \frac{k_T T_0}{k_E E_0};\ \ \beta = (k_E V E_0)^{-1};\ \ \epsilon = \frac{Rg_T}{T_0} = \frac{Rg_E}{E_0} \tag{8}$$

Here T_0 and E_0 are the background concentrations of TGF-β and EGF at the center of the device, respectively; g_T and g_E are the gradients of TGF-β and EGF, respectively; $V = 4\pi R^3/3$ is the volume of the spherical cell; and M_0 is the total number of M and M* molecules in the cell, which is constant. Setting ϵ directly from the experiments, and η to produce a stronger response with a TGF-β alone than with an EGF gradient alone as in the experiments, we find that there is a range of β values for which this simple model exhibits antagonism. An example is shown in Figure 4.4 B, and more generally, antagonism occurs for the following conditions,

$$\begin{aligned} \beta &< \sqrt{\eta(1+\eta)}\forall_\eta < 1 \\ \beta &< \sqrt{(1+\eta)}\forall_\eta \geq 1 \end{aligned} \tag{9}$$

The intuitive reason that antagonism occurs at small β is that small β corresponds to strong conversion rates of M to M*. This means that most molecules are in the M* state, i.e, the pathway is close to saturated. With only one gradient signal, the pathway is not yet fully saturated, and there are more M* molecules produced in the front of the cell than in the back. However, with both signals, the pathway becomes saturated, and the number of M* molecules is close to its maximal value in both halves, leading to a reduced difference ΔM^*.

The mathematical model gives the SNR, and while it is reasonable to assume that CI is a monotonically increasing function of the SNR [88], we would like to make predictions for the CI and its associated statistics directly. To do so, we develop a simulation of the cell response based on the mathematical model. We explicitly simulate the reactions in Eqs. 3-5, where T and E are modeled as continuous concentrations, and M/M* is modeled as a fixed number M_0 of discrete molecules uniformly distributed around the surface of a circular cell, as illustrated in Figure 4.4 B (We show in the Supplementary information that our results are similar to a spherical cell doing a biased random walk in 3D). The direction of movement θ is chosen according to the distribution of M^* on the surface, and the cell moves at a constant speed till the next reaction takes place. We calculate the CI from the simulated trajectory in the same way it is calculated in the experiments (Eq. 2). Using the same parameters ϵ, η, and β, and fixing M_0 to calibrate the CI to the TGF-β case

in the experiments, we find that our simulation results match the experimental results and successfully produce the observed antagonism (Figure 4.4 C and D).

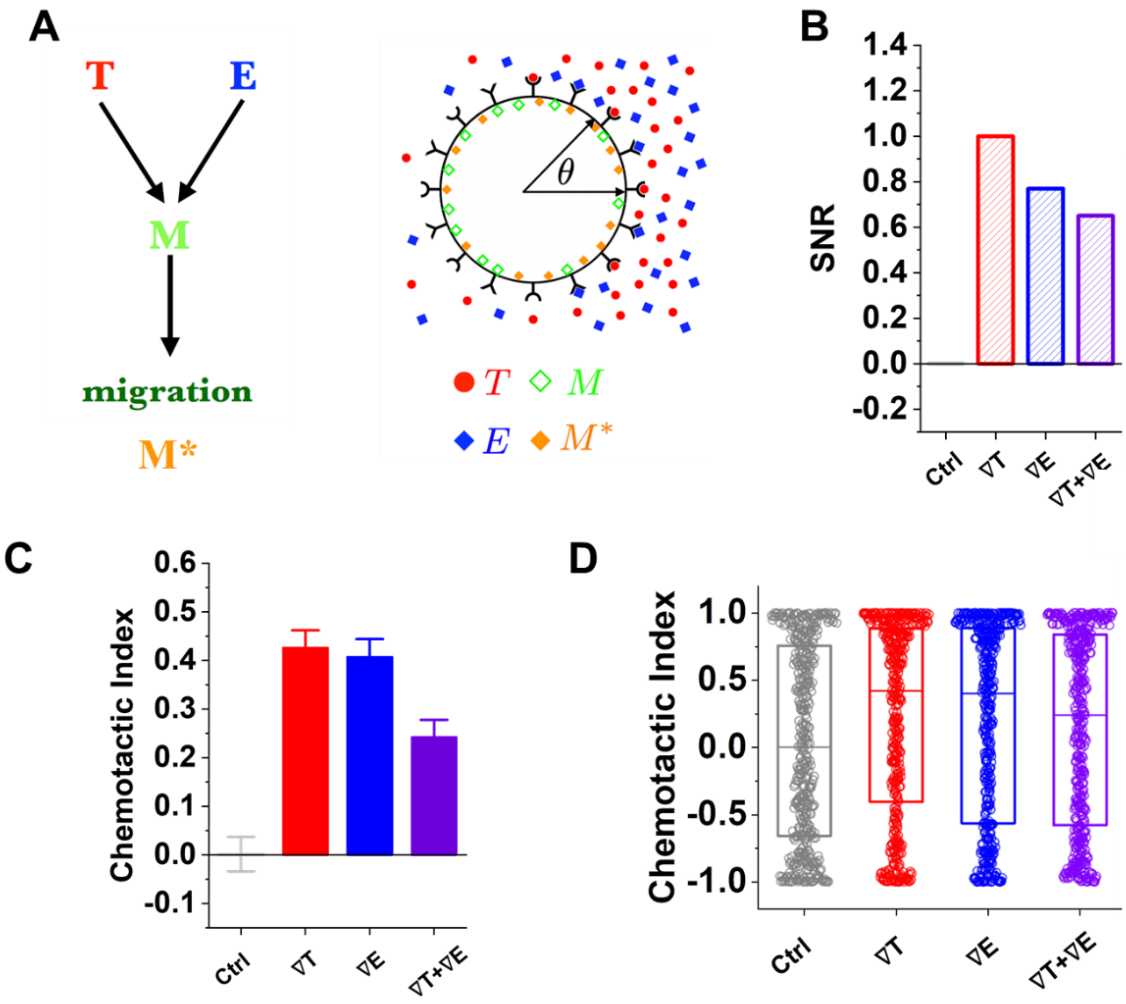

Figure 4.4. Mathematical model explains antagonism by saturation of common pathway component. (A) Schematic of model. T, TGF-β; E, EGF, M, common component; M*, activated form. (B) Signal to noise ratio (SNR) is lower for combined gradients than individual gradients (antagonism). (C,D) Simulation of model reactions reproduces experimentally observed antagonism in chemotactic index (CI) at level of medians (C) and distributions (D).

4.3.4 Model predicts that directional bias decreases as signal background increases

To evaluate the hypothesis that saturation of a common pathway component causes the antagonism, we develop two experimentally testable predictions using the model. Both predictions are based on the fact that saturation presents a tradeoff: the benefit of adding an EGF gradient to the TGF-β gradient is that it presents a stronger directional cue; the cost is that it pushes the number of activated molecules on each side of the cell closer to its maximal value and therefore takes the difference closer to zero. The cost wins, causing the antagonism. This intuition implies that if a uniform EGF signal is used instead of the EGF gradient, then the benefit is removed, and the CI should be further reduced. Indeed, the simulation results in Figure 4.5 A and C (black) show that the CI is significantly suppressed when adding a uniform EGF background concentration to the TGF-β gradient.

We test this prediction in the experiment. MDA-MB- 231 cells are exposed to 50 nM/mm of TGF-β gradient in the presence of a uniform 400nM EGF background concentration. We see in Figure 4.5 B and D (black) that the CI is significantly reduced, as predicted by the simulation. Because TGF-β and EGF bind to different receptors, this result implies that neither receptor is being saturated. Instead, it supports the hypothesis that saturation occurs at a common component downstream.

The previous result does not rule out the possibility that the EGF pathway specifically represses the TGF-β pathway to create the antagonism. To disambiguate the saturation mechanism from the possibility of repressive crosstalk, we consider adding to the TGF-β gradient a uniform background concentration of TGF-β instead of EGF. The intuition behind the saturation mechanism still implies that the CI should decrease, and indeed the simulation results in Figure 4.5 A and C (dark red) show that the CI is significantly suppressed when adding a uniform TGF-β background concentration to the TGF-β gradient. We also test this prediction in the experiment. MDA-MB- 231 cells are exposed to 50 nM/mm of TGF-β gradient in the presence of a uniform 200 nM TGF-β background concentration. We see in Figure 4.5 B and D (dark red) that the CI is significantly reduced, as predicted by the simulation. This result further supports the hypothesis that the antagonism is not due to repressive crosstalk, but rather due to the saturation of a common pathway component.

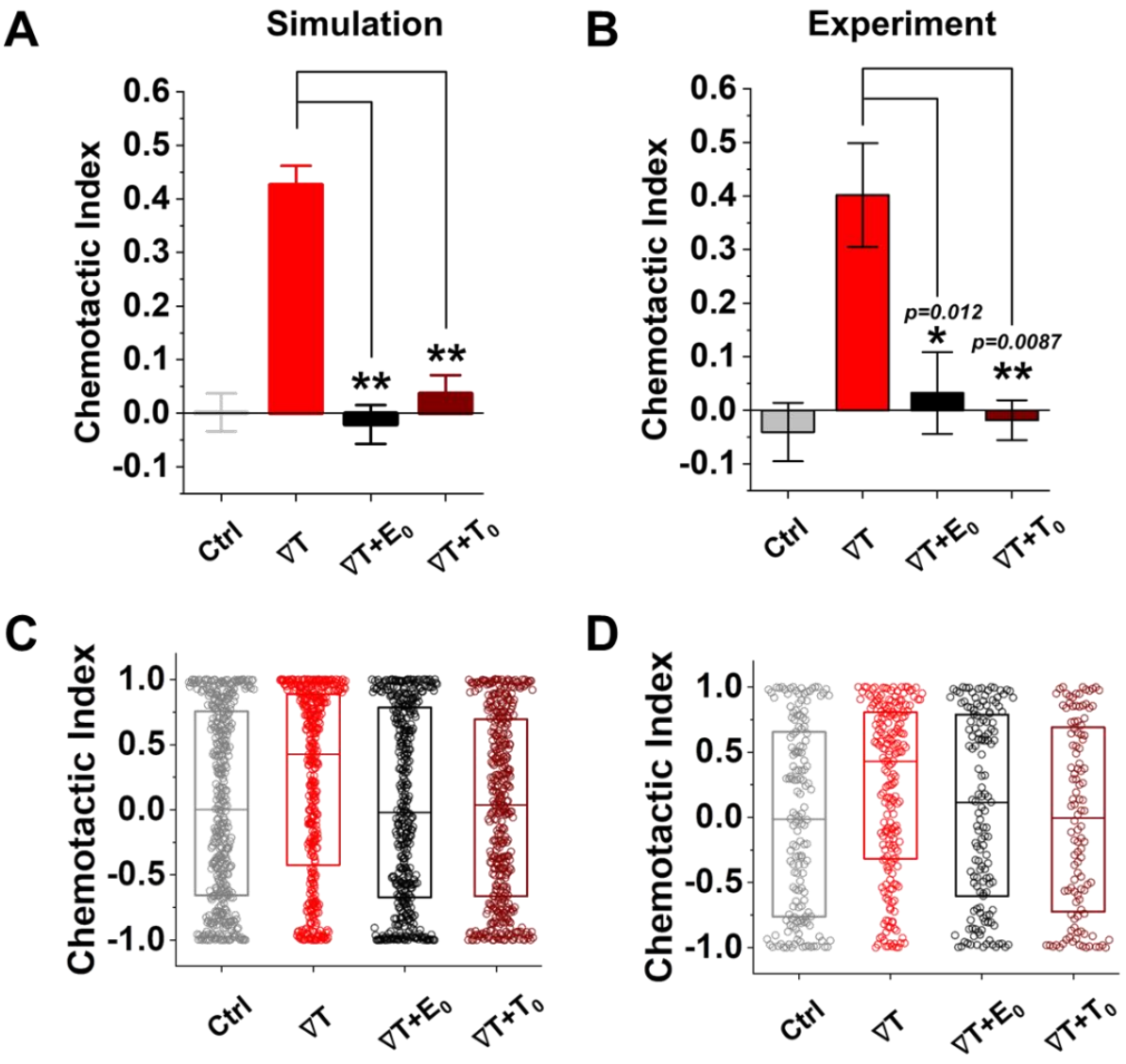

Figure 4.5. Effect of signal background on the chemotaxis up a TGF-β gradient. Chemotactic index (CI) from (A) simulation and (B) experiment show that chemotaxis up TGF-β gradient is highly suppressed with the addition of a uniform background concentration regardless the signal type. CI distributions of all trajectories of (C) simulation and (D) experiment are comparable. ;n≥3. Bar; mean ± S.E. *: p<.05, **: p<.01 (Student t-test). Dot; CI from a single trajectory. Box: quartiles with a median line in the middle of the box.

4.3.6 The antagonism is observed during chemotaxis of a different cancer cell type

Our biophysical framework makes predictions about chemotaxis in response to multiple cues, without specifying the cell type. Indeed, invasion in response to a chemical gradient is ubiquitous across mammalian cancer cell types, including pancreatic cancer cells [121]. To evaluate the cell-type dependency of the antagonism, we investigate multiple-cue chemotaxis in pancreatic cancer cells. eKIC is used in this study, which is a murine pancreatic cancer cell line. eKIC is driven by the genetically engineered mouse model having Kras and p16 mutations showing epithelial phenotype [122, 123]. The cell line is known to be responsive to TGF-β sensitively, showing invasion features [123]. First, we evaluate the migratory behaviors of eKIC in the chemotaxis platform as a control, excluding any growth factors. The trajectories show an unbiased U-shaped CI distribution, as shown in Figure 4.6 (gray).

Then, we expose a single cue of the TGF-β gradient and EGF gradient. We find that the eKICs are highly responsive to both the TGF-β gradient and EGF gradient (Figure 4.6, red and blue). Indeed, the CI values are significantly enhanced in both gradient groups compared to the control group. Interestingly, we observe the antagonism in eKIC in the presence of the combined TGF-β and EGF gradients: the CI is significantly lower than the CIs of both groups of a single gradient , and the CI values of eKIC trajectories are distributed in a similar trend with control (Figure 4.6, purple). The antagonism induced by combined gradients of TGF-β and EGF suggests that the saturation mechanism also applies to the pancreatic cancer type. Although further research should be conducted, the present results suggest that the pathway saturation is generic, applying across many types of chemotaxis. The chemotaxis is critically moderated by not only the environmental cues but also the intrinsic cell capability to process information within an inherently limited channel. Specifically, genetic mutations commonly observed in the cancer cells are highly relevant to exhibit the invasion process with specific signaling pathways such as Snail and Twist [124]. Yet, the present results show that the cell response could be illustrated with the predictions from our framework regardless of the cancer type, implying the antagonism is not cancer type-specific signaling effect.

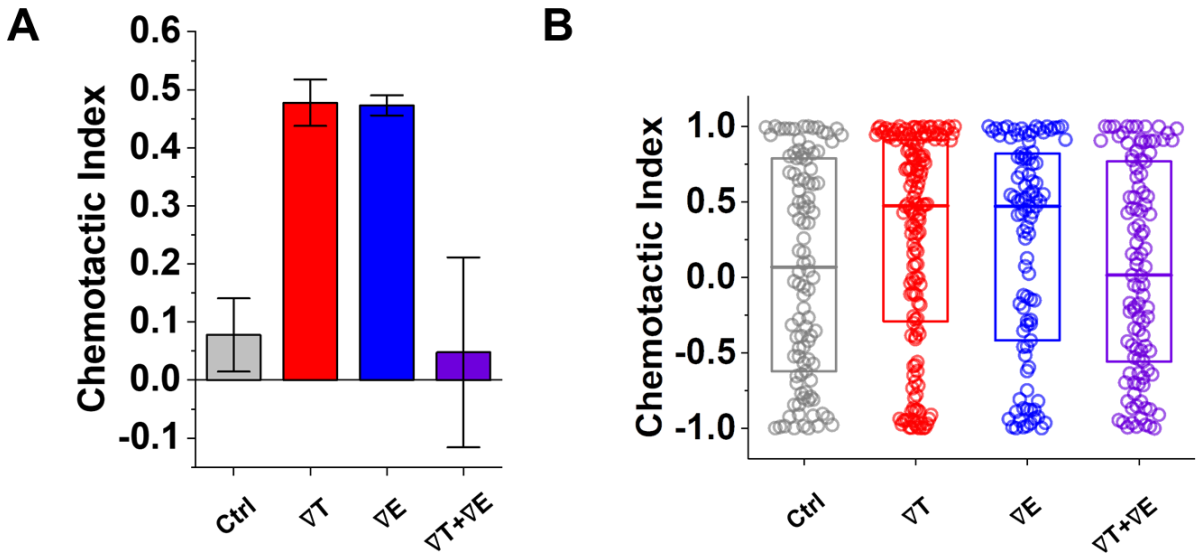

Figure 4.6. Antagonism of TGF-β gradient and EGF gradient in pancreatic cancer cells. (A) Averages of medians of chemotaxis index (CI) in control, 10nM/mm TGF-β gradient (∇T), 200nM/mm EGF gradient (∇E), and combined gradients of 10nM/mm TGF-β and 200nM/mm EGF (∇T+∇E), and (B) CI distribution of all trajectories ;n≥3. Bar; mean ± S.E. *: p<.05, (Student t-test). Dot; CI from a single trajectory. Box: quartiles with a median line in the middle of the box.

4.4 Discussion

The present results elicit the antagonism of the combined signals, TGF-β and EGF gradients, in chemotactic accuracy of cancer cells. The chemotactic accuracy of the cancer cells showed significant suppression when the TGF-β and EGF gradients were simultaneously exposed to the breast and pancreatic cancer cells in the in vitro chemotaxis platform. Both growth factors have been identified to regulate cell invasiveness and motility (2, 31, 32). In particular, the TGF-β has been well recognized to promote epithelial-mesenchymal transition, which is a critical step in cancer invasion (23, 31). The role of TGF-β in stimulating cancer progression and invasion has been considered as a cooperative effector when it combines with the other growth factors. (20, 22). Uttamsingh. et al., (20) reported that the roles of TGF-β and EGF-mediated signaling pathways incorporate synergistically in inducing cell invasion and migration. However, the synergistic effect of TGF-β with EGF is a result of the intrinsic capability relevant to cell motility, not fully

addressing the cell chemotactic response. On the other hand, our results showed the combined effect of the signals specifically for the cell chemotaxis as a systematic response. Indeed, cell chemotaxis is regulated by not only the intrinsic motility but also the physical aspects (14, 33, 34). We observed the antagonism of TGF-β and EGF gradients mainly in the cell chemotactic accuracy, while not in the motility. Moreover, the antagonism was shown in the highly noisy environment in detecting the signals, indicating the biophysical aspect of the chemotaxis. Therefore, the antagonism in this study is a novel discovery, suggesting the necessity of a quantitative approach to multiple cue migration studies.

To understand the antagonism, we proposed the biophysical framework with a simple mathematical model and simulation by suggesting the saturation of a common pathway component M*. In the framework, each growth factor activates an intracellular molecule, and these molecules compete for binding to a motility factor, M and helping it to convert to a molecule responsible for cell migration M∗. The simple competitive binding model enables several surprising predictions. First, the simultaneously exposed TGF-β and EGF gradients can induce the chemotaxis weaker than the individual responses, addressing the antagonism found in the experiment. Also, the higher background noise causing the saturation of the motility factor elicits the loss of chemotactic accuracy in the cell response. The predictions were well validated by the experiment with strikingly similar results, suggesting the capability of the new framework to encompass many types of chemotaxis.

The biophysical framework demonstrates the combined action of multiple cues simply by focusing on the functional molecules which directly regulate cell chemotaxis. The chemotaxis is a systematic activity of intrinsic cellular responses, including actin polymerization and organization, cytoskeleton dynamics, and adhesion (2, 7, 8). Recent advances have reported several signaling pathways regulating chemotaxis (9, 10, 35, 36). The localization of the relevant proteins in either the leading edge or the rear regulates the cell polarity and motility. Such proteins are activated when the environmental signals are detected and regulate the F-actin polymerization, myosin, microtubules, and adhesion. The complex process is illustrated simply in our model by using the common pathway components M and M*. In this matter, our framework provides new insights to elucidate the cellular process in a simple and quantitatively testable way.

Although the biophysical framework is capable of illustrating the antagonism shown in the experiment, further research could be performed to strengthen this concept. In the signaling

networks, activation of intracellular proteins such as M by detecting the signals might have different kinetics, which could be another potential mechanistic explanation. Moreover, the present framework may limit the explanation in a mode of the migration. The physical constraint driven by ECM regulates the migrating features as well. Since the chemotactic response and relevant signaling pathway inducing the chemotaxis could be varied depending on the mode of the migration (34, 35), the model may be improved further by considering the modes highly regulated by the physical confinement. Some mechanistic study may also improve the concept in integrating the biophysical framework with the signaling networks for chemotaxis by finding the potential molecules corresponding with M and $M*$.

5. THE EFFECT OF A CONVECTION-DRIVEN SIGNAL ENVIRONMENT TO DIRECTED CELL MIGRATION

5.1 Introduction

Directed cell migration is a crucial step in various cell processes, including cancer metastasis, the immune process, and angiogenesis. For decades, studies have sought to understand the cell responses to environmental signals that induce directed cell migration to develop plausible therapeutic strategies for various diseases, specifically cancer metastasis. Recent studies have recognized that cells are capable of sensing both chemical and mechanical signals in regulating their migratory behaviors in the microenvironment. [14, 29, 66] The tissue microenvironment, which is highly complex, is composed of heterogeneous cell types, various chemical cues, ECM components, and interstitial fluid. Interstitial fluid flow is caused by pressure variance, which develops in a circulating nature. Meanwhile, the tumor microenvironment carries distinct features; leaky vasculature and abundant ECM compartments increase interstitial fluid pressure (IFP) and develop uncertain pressure variance, causing aberrant features of interstitial flow. [125] Interstitial flow plays an essential role in the pathological processes of cancer. [126, 127] It involves the transport of nourishment sources and chemical signals by shaping the abnormal signal environment that promotes cancer progression, metastasis, and drug resistance. Moreover, recent studies have recognized that cancer cells are capable of recognizing interstitial flow as an environmental signal that regulates directed cell migration. In this sense, cells sense and decipher the complex environmental cues of both the chemical gradient (chemotaxis) and interstitial flow (rheotaxis) for stimulating the directed migration. To advance our understanding of cell response in the complex microenvironment, acknowledgement of the role of interstitial flow in shaping the complex signal environment is crucial.

Cancer cells are exposed to the complex signal environment due to desmoplastic stroma, leaky vasculature, and overgrowing tumor cells. Multiple cytokines, including transforming growth factor-beta (TGF-β), are secreted by cancer-associated stroma that stimulate a cancer invasion in diverse cancer types. [4, 24, 111, 128, 129] In some tumor types, such as pancreatic adenocarcinoma, it has been observed that increased IFP at the central location of the solid tumor alters the pressure variation in the interstitial regions. [129-131] The increased IFP at the tumor core causes aberrant interstitial flow from the tumor core to the periphery. [131, 132] Indeed, the

IFP variation in the interstitial space is highly heterogeneous. [132] The regional variation of IFP results in generating various scenarios in developing the signal environment depending on the tumor region, cancer types, and patients. [127] The IFP differences between the core and the periphery cause an increased flow rate toward the lymphatic vessel, causing increased metastatic potential. [133, 134] Abundant ECM components and a high density of cancer/stroma cells impedes the flow perfusion in the interstitial region, causing a slowed interstitial flow of < 1 μm/s. [125, 132] Due to the complexity involved, the signal environment that is induced by interstitial flow is largely unknown. Chemical signals are transported in the tumor microenvironment through both advection and diffusion. The Péclet number (Pe), which is defined as a ratio of the advection mass flux to diffusion mass flux, indicates that convection is not negligible when considering the reported interstitial flow range of 0.1–10 μm/s. [126, 127, 135]

Interstitial flow plays an important role in cell physiological and pathological processes as a mechanical signal itself. Indeed, recent studies have recognized that cancer cells are capable of sensing interstitial flow and activating signaling pathways to regulate directed cell migration. [29, 79, 136, 137] Polacheck et al. [29] reported that the directed migration of breast cancer cells is stimulated by interstitial flow (0.5 and 3 μm/s). Their study showed that the cell trajectories are mostly aligned to the flow streamline. The direction of cell movement was determined by the competing mechanisms between autologous chemotaxis and Focal Adhesive Kinases (FAK) activation. Cells under autologous chemotaxis can sense the flow signal via self-secreting chemokine detection with CCL7 receptor activation, and the cells are induced to move in the flow's direction. [79] By contrast, the cells' direction is biased toward the upstream direction of the flow through the FAK activation. [130, 138] The FAK are signaling networks that are governing mechanotransduction through integrins on the cells, and they are highly relevant to mechanical stress sensing. Although it is still poorly understood how shear stress activates cell mechanotransduction, recent studies have begun exploring the signaling cascades of shear stress stimulation in intracellular signaling transduction. [20, 104, 139] Interestingly, the downstream networks of shear stimulation overlap with the chemotaxis signaling transduction that regulates actin cytoskeletal dynamics, which are thought to manipulate the cell response to bias movement. [139]

Despite recent advances in understanding the effect of interstitial flow as a mechanical signal that stimulates directed cell migration, it is still largely unknown how signal environment

influences cell response due to its complex nature. In particular, little is known about the combined effect of the chemical gradient and interstitial flow. In this study, we investigated the effect of interstitial flow on the chemotactic environment of pancreatic cancer cells and the cell response to the signal environment. In our previous studies (chapter 4), we showed that pancreatic cancer cells are responsible for the TGF-β gradient with enhanced directional accuracy and motility. Here, we applied interstitial flow in the cells that were stimulated by the TGF-β gradient. The driving hypothesis of the study is that directed cell migration results from a balance between environmental signal stimulation and a cell's innate ability of signal sensing and processing. We evaluated the hypothesis by engineering the microenvironment *in vitro* to develop a TGF-β concentration gradient that presents interstitial flow. We firstly investigated the transport behavior of TGF-β in the presence of interstitial flow, followed by applying interstitial flow 1) from source-to-sink and 2) from sink-to-source channels to combine the chemical gradient with the flow signal.

5.2 Materials and methods

5.2.1 Cell cultures and reagents

KIC is a murine pancreatic cancer cell line isolated from genetically engineered mouse model (GEM) of PDAC. The KIC cells were established from KIC mice in which *Kras* was combined with deletion of the *Ink4a* locus (*Ink4a/Arf*$^{L/L}$). [117, 118] In our prior research [140], we showed that the KIC cells highly responsive to TGF-β increasing their invasion capability. These cells were maintained in RPMI 1640 with 2.05mM L-glutamine (GE Healthcare Bio-Sciences Corp., MA, USA) supplemented by 5% v/v fetal bovine serum (FBS) and 100 μg ml^{-1} penicillin/streptomycin (P/S). The cells were regularly harvested by 0.05% trypsin and 0.53mM EDTA (Life technologies, CA, USA) when grown to ~80% confluency in 75 cm^2 T-flasks and incubated at 37°C with 5% CO_2. Harvested cells were used for experiments, or sub-cultured while maintaining them below 15th passage.

5.2.2 Engineered microenvironment platform

In the chapter 3 and 4, we used a microfluidic platform composed of center, source, and sink channels. The platform was capable of exposing a linear concentration gradient in the center channel by diffusion excluding pressure variation. In this study, we engineer the pressure variance

between source and sink channels by facilitating the microfluidic platform so that the pressure driven flow is generated in the center channel. The hydrostatic pressure differences are controlled by applying the medium level differences between two channel reservoirs as shown in the Figure 5.1.

To apply the interstitial flow in a presence of TGF-β gradient, we fill out the source channel with 10nM of TGF-β while the sink channel is filled with normal culture medium and vary the hydrostatic pressure of each channel to control the flow rate of ~1μm/s. To achieve the boundary conditions (C_{source}=10nM TGF- β and C_{sink}= 0nM TGF-β) at the interface of the medium solution and collagen matrix, we apply consistent flow through the sink channel as Q_{drain}=40μl/h by connecting it with syringe pump (NE-1000-ES, New Era pump system, USA). We assume that the drain flow at the sink channel is not critically interrupted the interstitial flow at the center channel with relatively small area of the interface.

5.2.3 Characterization of the directed cell migration

Live-cell time-lapse imaging with an inverted microscope (Olympus IX71, Japan) was utilized to characterize the cell migration. A stage top incubator allowed maintaining the microfluidic platform at 37ºC with 5% CO_2 condition during imaging as described in previous chapters. [94] eKIC cells were captured every 5 minutes for 3 hours. The time lapse images were captured 3 hours after applying the growth factors to give an adjustment time for stable environmental condition. The bright-field time lapse images were segmented to analyze cell trajectories by using ImageJ. Cell region was determined by the image contrasts which provided clear boundaries between cells and background. Then, cell centroids were collected in the converted monochrome images. A collection of the centroids of cell areas at different time points were defined as a cell trajectory. In collecting cell trajectories, we rejected the cells under division and the stationary cells. This is because the dividing cells could affect for cell polarity [119] and the stationary cells could underestimate the cell movement characteristics. The stationary cells were defined when cells were moving less than the estimated cell diameters.

The directed cell migration is characterized by motility and directional accuracy. [94] The direction of the cell trajectories is analyzed based on the direction of environmental cues. We measure directional accuracy using the directional accuracy index (DAI)

$$DAI = \cos\theta \tag{10}$$

where θ is the angle between the net displacement of a trajectory and the environmental cue direction. The DAI is corresponding definition with CI in the previous chapters. A straight line connecting the initial and final points of a trajectory indicates a displacement. For the chemotaxis, the direction of environmental is along with the concentration gradient direction from low to high. When the interstitial flow is applied as an environmental cue, we compare the cell bias with upstream direction of the flow along with the flow streamline considering the recent studies reporting the cells were stimulated toward the upstream direction. [29] When both chemical gradient and interstitial flow are applied at the same time, the direction of environmental follows the chemical gradient direction. The DAI range is between -1 and 1. DAI = 1 indicates that the cell is perfectly biased to the environmental cue direction, whereas CI = 0 means that the cell is showing random motion. On the other hand, DAI=-1 indicates that the cell moves toward the completely opposite direction from the environmental cue. Thus, higher DAI indicates the highly accurate the cell biased migration. In an experimental trial, cells show distributed DAIs throughout the range of -1 to 1 due to the nature of cell response to the attractant. In the distribution, a median DAI represents a result from the trial. More detailed description about DAI is stated in the previous chapters [94]. Cell motility is defined as an instantaneous speed as also described in the previous chapters. Here, the cell path is taken from a trajectory where measurement is taken every Δt = 5 minutes.

5.2.4 Statistical analysis for experiments

All experimental controls were repeated at least three times and more than 30 trajectories were collected in an experiment. A trajectory was evaluated with quantified DAI and speed. To compare the chemotactic accuracy, the distribution of DAIs was reported in box plot with distribution of data points. A data point in the box plots indicates the metric of a cell trajectory. Averaged median values were statistically analyzed with student t-test with $p<0.05$ in Figure 5.2 and 5.5. Median values of the distribution were statistically examined with Mann-Whitney nonparametric test with $U <0.05$ in Figure 5.8.

5.3 Results

5.3.1 Pressure driven flow in the microfluidic platform

To investigate the cellular response to the complex signal environment comprising chemical signals with interstitial flow, we decoupled the combined signal environment into two parts: chemical signals with the TGF-β gradient and the flow signal. In previous chapters, we have shown that cancer cell chemotaxis is induced by TGF-β. Here, to explore the flow's effect on cell migration, we controlled the low Reynolds flow through the collagen matrix (0.5–3μm/s) that corresponded to the interstitial flow rate of the tumor's microenvironment. [13, 125]. In controlling the flow rate, we considered the Brinkman equation:

$$\nabla p_i = -\frac{\mu}{K}\bar{v}_f + \mu\nabla^2\bar{v}_f$$

where $\bar{v}_f$ is the average flow rate, μ is a dynamic viscosity, and K is the permeability of the culture medium in a type I collagen matrix of 2mg/ml. [13, 141] The pressure variance was applied between the source and sink channels by controlling the hydrostatic pressure levels of each reservoir, respectively. In the literature, the permeability K in a type I collagen matrix of 2mg/ml has been reported to range from 10^{-14}–10^{-13} m^2. [29, 137, 142]. To control the flow rate of ~ μm/s, we applied the pressure differences ΔP ($P_{source} - P_{sink}$) = ~2mmH_2O, adapting ∇p ~ 19.6 Pa/mm in the center channel 19.6 Pa/mm with the average K = 5×10^{-14} m^2 from the varied range. To verify the scale of the controlled flow rate, we measured fluorescent beads' (0.2μm diameter) trajectories. The results show that the average ± standard error of the collected particle velocities was 1.5 ± 0.048 μm/s. By using the measured value of the flow rate that was driven by the controlled pressure variance, permeability K for 2mg/ml type I collagen matrix was 8×10^{-14} m^2 with μ = 0.84cP of DMEM [13], which is comparable with previous studies. [29, 143]. In addition, the flow streamlines in the region of interest (ROI) in the platform where we tracked the cell migration were evaluated. The Brinkman equation was analyzed by the finite element model with Comsol Multiphysics simulation (Figure 5.1). We set the wall boundary in a slip condition, where boundary conditions on the channel interfaces (source-center and center-source) were set to constant pressure differences in 19.6 Pa/mm. In the simulation result, we confirmed that the streamline of the flow was aligned in parallel to the source-to-sink direction and not interrupted by the platform geometries in the ROI.

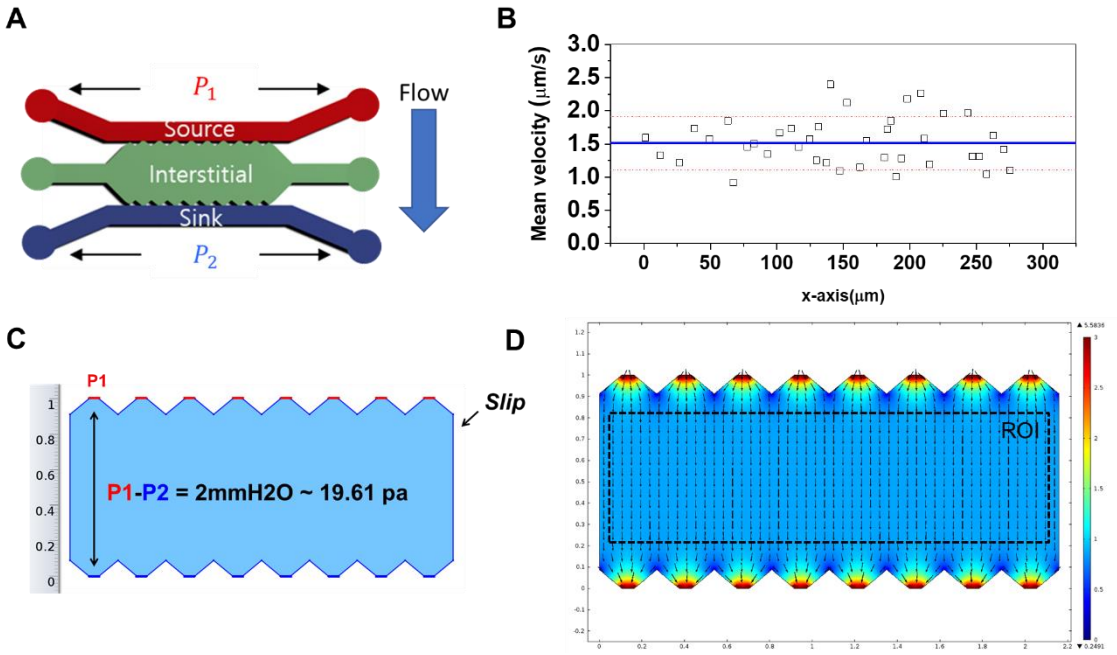

Figure 5.1. Illustration of microfluidic platform with pressure driven flow and computational simulation results. (A) Schematic description of engineered pressure driven flow. (B) Measurement of the flow velocity driven by ∇p=19.6Pa/mm through red-fluorescent PS bead (0.2μm) tracking. Blue line indicates an average and red dash line is standard deviation. (C) COMSOL simulation models mimicking the microfluidic platform and boundary conditions (D) The flow streamlines (arrows) in ROI

5.3.2 Interstitial flow stimulates the directed cell migration

The next step was evaluating the effect of interstitial flow when excluding the chemical signals. eKIC cells that were deposited in the type I collagen matrix were exposed to the pressure-driven flow controlled as ~1 μm/s. Interestingly, the directional accuracy denoted as DAI showed biased features toward 1, indicating the cells followed the upstream direction of the flow. The biased features of the cell DAIs that were exposed to interstitial flow showed significant changes in the average median compared with the control (Figure 5.2B). However, the biased accuracy in the flow stimulation was not stimulated as much as that of the TGF-β gradient of 10nM/mm close to 0.5. The flow enhanced the cell speed slightly compared to the control, but it was not as significant as the TGF-β gradient (Figure 5.2C). The results support previous studies showing the effect of shear flow on the cell migration, even without any growth factors contributing to cell motility. [29] The cell migration followed the upstream direction of the flow, implying that the

flow activated mechano-sensing of FAK instead of autologous chemotaxis in inducing directed cell migration. [29, 138]

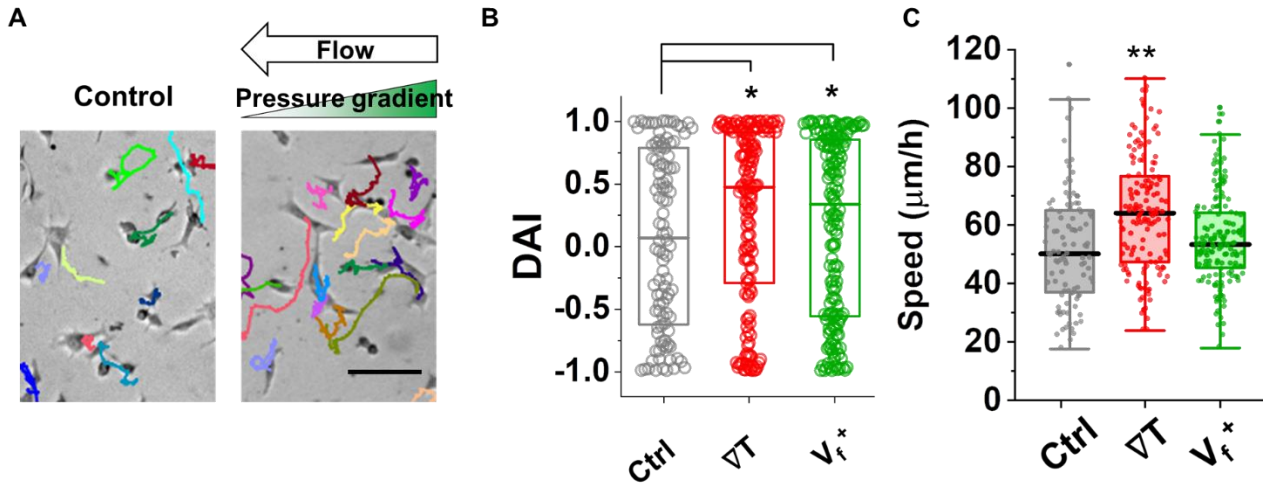

Figure 5.2. The effect of the interstitial flow in the directed cell migration of eKIC. (A) Micrograph of eKIC in control and pressure-driven flow with trajectories. (B) Directional accuracy index (DAI) distribution of collected cell trajectories of control(Ctrl), 10nM/mm TGF-β gradient (∇T), and the interstitial flow (V_f^+). Box: quartiles with a median line in the middle of the box. Dot: the corresponding metric from a single trajectory. * : p<.05 (Student t-test with average of median DAIs) (C) Speed distribution of collected cell trajectories of ctrl, ∇T, and V_f^+. Box: interquartile range (IQR) ± 1.5 IQR whiskers with a mean line in the middle of the box. ** : p<.01 (Student t-test with average of median speeds)

5.3.3 Interstitial flow alters the signal environment of cancer cells' surroundings

To understand the convection-driven signal environment to which cells are exposed, we examined the TGF-β transport in the microenvironment, where various chemical signal factors, such as TGF-β, regulate cancer cell invasion and migration. The chemical signals are transported in the microenvironment via pressure variation, which causes interstitial flow. Under the influence of abnormal IFP variation, the signal environment is highly heterogeneous, depending on the region. Here, we considered the TGF-β transport dynamics in the 2mg/ml type I collagen matrix in the presence of interstitial flow. TGF-β was selected to stimulate the directed cell migration because it has been widely recognized as a strong chemoattractant, as shown in previous studies.

[4, 94] Moreover, eKIC, were highly responsive to the TGF-β by showing enhanced invasion capability [123], and enhanced directional accuracy (see chapter 4). To illustrate the chemical signal environment that is driven by convection, we examined the Pe, which implied which mode of transport was dominant in the system as follows:

$$Pe = v_f L_c / D$$

where v_f is the flow rate, L_c is the characteristic length, and D is the diffusivity. In the higher Pe >> 1 environment, the chemical signals transport through convection, whereas lower Pe << 1 derives diffusion-dominant transport features. In considering the estimated diffusivity of TGF-β ($D_{TGF\text{-}\beta} = 1.5\times10^{-10} m^2/s$) [144] and Lc=100μm representing general spacing between microvessels [135], the Pe numbers varied from 0.33 to 2, and the reported range of the interstitial flow rate was 0.5–3μm/s in the tumor microenvironment, indicating that both diffusion and advection command the transport of TGF-β.

We then modeled the simplified signal environmental conditions to exhibit the effect of the flow in the chemical environment's features. In determining the concentration profile, the governing equation was analyzed with constant flow rates, which varied from -3 to 3μm/s, while we denoted that the flow was positive when moving from a higher to a lower concentration.

$$\frac{\partial C_i}{\partial t} = \nabla \cdot (\underbrace{D_{eff} \cdot \nabla C_i}_{Diffusion} - \underbrace{v_f \cdot C_i}_{Advection})$$

For simplicity, the maximum concentration 1 was assumed, where the dense stroma region consistently secretes the upregulated TGF-β, while the minimum concentration 0 ($C_{source} = 1$ and $C_{sink} = 0$) was assumed as modeling the region near drainage of the lymphatics. The initial condition $C_0 = 0$ was applied, and the boundary conditions varied in two different scenarios: i) $\Delta p = p_{source} - p_{sink} > 0$ and ii) $\Delta p < 0$ (instead of using the actual concentration). Scenario i) illustrates that the concentration gradient direction was parallel to the pressure gradient corresponding with the upstream flow, whereas the concentration gradient direction was opposite the pressure gradient that was aligning with the downstream flow direction in scenario ii). At a steady state, the concentration gradient of TGF-β was developed as a linear profile with $v_f = 0$ where the diffusion was dominant. Once the flow was applied, the gradient profiles altered to the nonlinear exponential depending on the direction of the flow and the Pe (Figure 5.3). When comparing it with the linear profile, two distinct changes were observed by applying the advection. First, the gradient becomes shallower in most regions, but the edge is near the boundaries. When the flow direction is aligned

from source to sink ($\Delta p > 0$), the flow carries the molecules and helps deliver them to the affected region, which increases the background concentration. In addition, the gradient in the middle is shallower, whereas it is highly steep near the drainage area. However, the flow resists delivering the signal in the opposite direction ($\Delta p < 0$). The background concentration of the signal is relatively low while the gradient is growing and becoming quite steep near the source. The results imply that diverse scenarios can be developed in the tumor microenvironment, which highlights the importance of studying how cells behave in the complex signal environment.

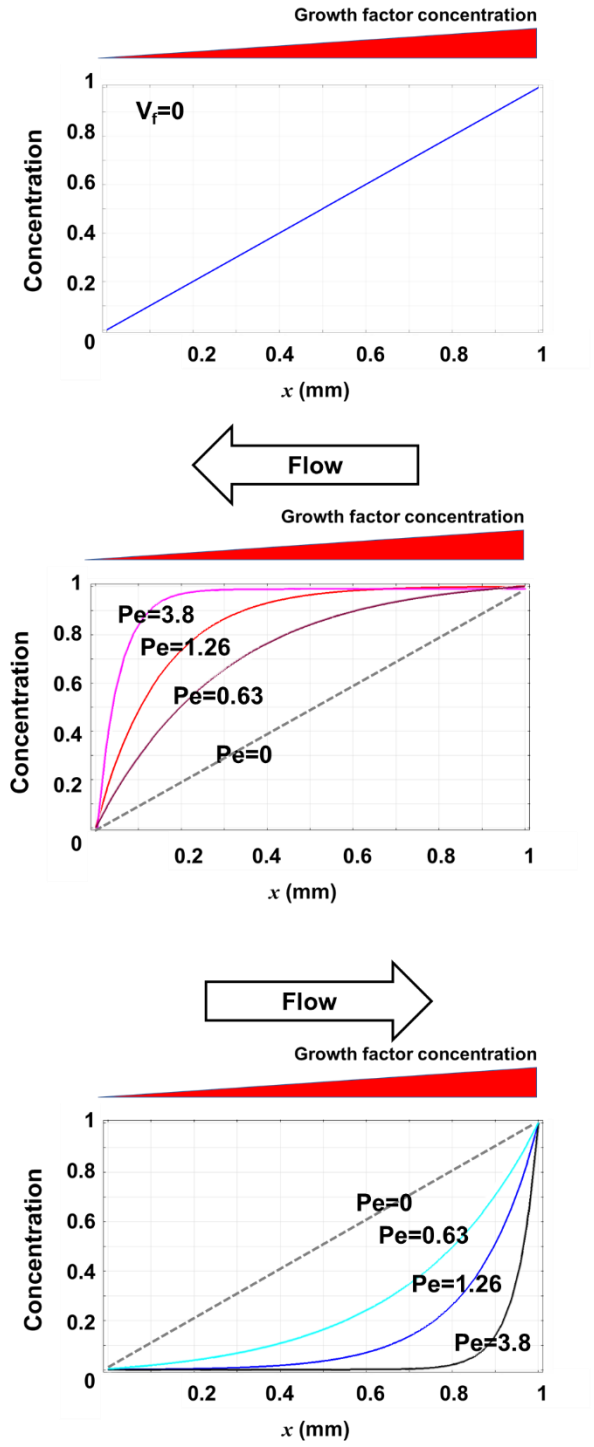

Figure 5.3. Concentration profiles of TGF-β in presence of the interstitial flow depending on Péclet number (Pe).

5.3.4 The convection-driven signal environment enhances directional accuracy to a limited degree

The convection-driven signal environment is complex because the flow alters the gradient profiles in the non-linear gradient. Moreover, cells can sense the flow as an environmental signal. Here, the effect of the combined stimulation for the directed cell migration was investigated by exposing the convection-driven TGF-β gradient to the eKIC cells in the engineered microfluidic platform. In our biophysical framework (see chapter 4), the cell capability of signal processing can be governed by the limited number of common molecules regulating the directed cell migration. Meanwhile, the signaling transduction for the flow stimulation has been recognized to regulate actin cytoskeleton dynamics by manipulating intercellular signaling molecule activation, which overlaps with chemotaxis stimulation. [139] Thus, we hypothesize that the combined signal environment of the convection-driven chemical gradient results in limited stimulation of the directed cell migration based on the physical capability of the cells. To study the hypothesis, we investigated the directed migration of eKICs by exposing the combined signal environment in the scenarios Pe ~ 1 ─ i) $\nabla C_{TGF\text{-}\beta} \times \nabla p > 0$ (denoted as $\nabla T + v_f^+$) and ii) $\nabla C_{TGF\text{-}\beta} \times \nabla p < 0$ (denoted as $\nabla T + v_f^-$), which show that the migration of eKICs was biased toward the directions of either ∇T of 10nM/mm or the flow upstream (v_f^+) of 1μm/s. Pe ~1 was achieved by v_f ~ 1μm/s when $D_{TGF\text{-}\beta}$ was estimated as 1.5×10^{-10} m^2/s. [142] To apply the boundary conditions of the sink ($C_{sink} = 0$) and source channels ($C_{source} = 0$), the additional drainage flow of 40ul/h was applied in either the sink channel ($\nabla T + v_f^+$) or the source channel ($\nabla T + v_f^-$).

Prior to exposing the TGF-β, we simulated the TGF-β transport by using 10kDa FITC-dextran to verity the TGF-β concentration profiles in the engineered platform. We mimicked the TGF-β transport 2mg/ml type I collagen by considering the hydrodynamic radius: $R_h = 2.1$nm for 10kDa dextran and $R_h = 2.3$nm estimated for TGF-β. [93] Consequently, the fluorescence intensity profiles of the dextran in the center channel in Figure 5.4 fit the exponential curve, which is closely comparable with the FEM simulation results of the nonlinear profiles found in Figure 5.3.

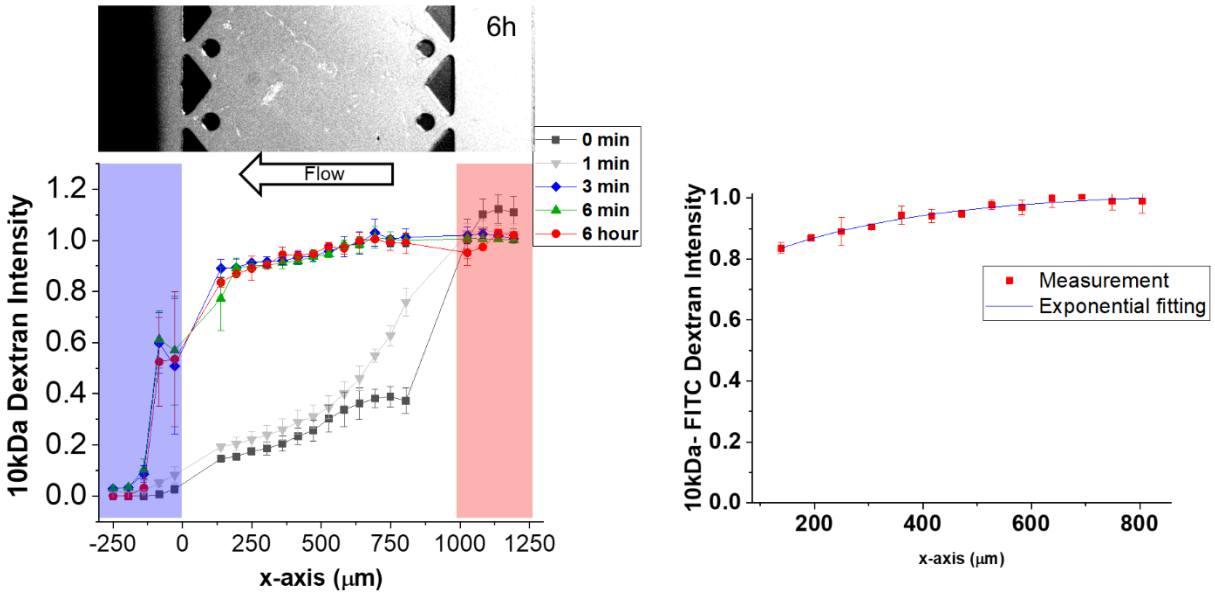

Figure 5.4. Normalized FITC-dextran fluorescence within the center channel in presence of the flow representing the signal environment of $\nabla T + V_f^+$. (Left) The fluorescence micrograph with the quantified intensity graph of 0 to 6h. Blue region indicates sink channel while region indicates source channel. (Right) The exponential fitting with R^2=0.926 on the quantified intensity at 6h.

Next, we exposed the engineered signal environment of TGF-β combined with the flow to eKIC cells. To do so, we evaluated the directed migration of the cells that were exposed to $\nabla T + v_f^+$. As shown in Figure 5.5 (purple), the motility of the eKIC cells was significantly enhanced compared to the control groups. The median of the speed distribution reached 72μm/h. Additionally, the directional accuracy was enhanced toward the signal direction that was corresponding to the TGF-β gradient in both cases. The DAI was observed as ~0.3 in $\nabla T + v_f^+$, which was similar to the flow-only case. Although we exposed the two stimulations along the same direction, the directional accuracy did not improve in either case; this may have been due to the shallower gradient, which could reach the physical limit of cell sensing. However, it was difficult to decouple the combined signal environment to compare it with results from each individual stimulation. Next, the cells were exposed to the signal environment of $\nabla T + v_f^-$ (Figure 5.5 [Orange]). The motility was significantly enhanced with statistical significance to the control. The cells were slightly biased toward the chemical gradient direction with DAI ~0.115. Because of the subtractive stimulation that was caused by applying the flow in the opposite direction, the

quantitative TGF-β gradient might have had a stronger effect than the flow signal, even though the gradient strength became shallower (by approximately 20%) due to the flow. However, it is still largely unknown whether the cause was non-linearity in the TGF-β concentration profiles or if there are other reasons given the diverse environmental signals that were emulated in the results.

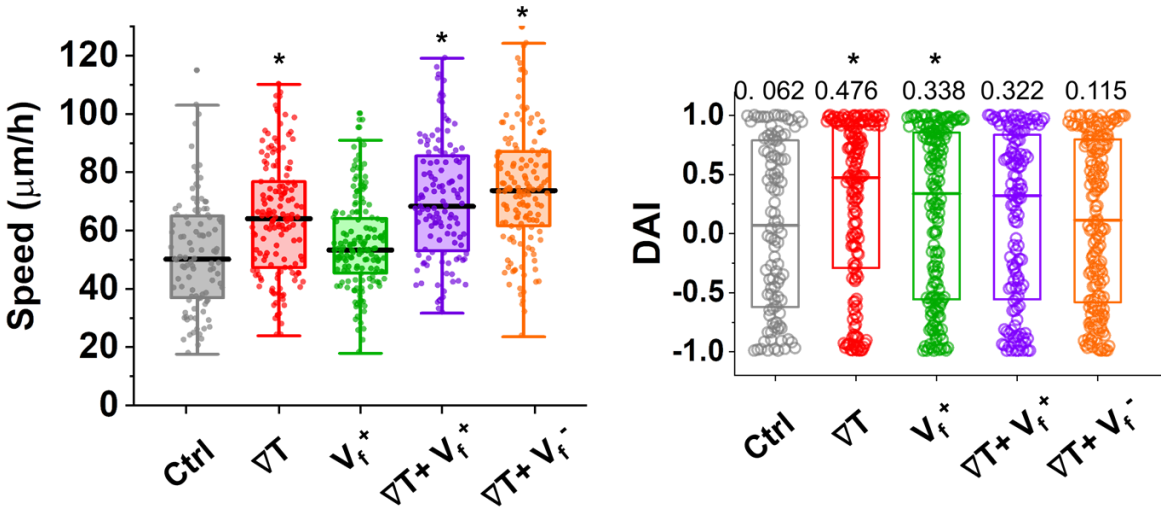

Figure 5.5. Directed cell migration characteristics of eKIC. Speed (left) and DAI (right) distributions of all collected trajectories of eKICs in control (Ctrl, grey), 10nM/mm of TGF-β gradient (∇T, red), 1μm/s of the flow from the source to sink channels (V_f^+, green), 10nM/mm of TGF-β gradient with 1μm/s of the flow from the source to sink channels (∇T+ Vf+, purple), and 10nM/mm of TGF-β gradient with 1μm/s of the flow from the sink to source channels (∇T+ Vf -, orange). n≥3 for all cases. Speed (left); Box: interquartile range (IQR) ± 1.5 IQR whiskers with a mean line in the middle of the box. * : p<.05 (Student t-test with average of median speeds) DAI (right); Box: quartiles with a median line in the middle of the box. The numbers on top indicate medians. Dot: the corresponding metric from a single trajectory. * : p<.05 (Student t-test with average of median DAIs)

To interrogate the effect of the combined signals, the cell response to the shallow gradient was further assessed. Due to the advection, the concentration gradient of TGF-β was refined as a non-linear exponential, whereas the linear gradient was formatted without the flow. Although the exponential profile (either $\nabla T + v_f^+$ or $\nabla T + v_f^-$) provided a steeper gradient near the boundaries (source or sink), tumor cells were typically seated in the region between the boundaries in the tumor microenvironment. In this sense, interest was in the middle region where cells were exposed to a shallower gradient. Many types of cells, including cancer cells, are capable of sensing shallow

gradient signals. Indeed, studies on the sensory precision threshold for *Dictyostelium* [145, 146] and cancer cells [79, 94] have elucidated that cells can sense only ~1% of concentration differences across the cell body. However, a cell's ability to sense spatial gradient signals has a physical limit. The cell surface receptor–ligand-binding dynamics and molecule diffusion command the cell to have precision sensing in a noisy environment. [146] Accordingly, we examine the gradient signal environment within the center channel to roughly determine where the environmental condition meet the physical detection limit [25, 94]. The percent change of the chemical concentration across the cell body was determined as $\bar{p}[\%] = \frac{ga'}{\bar{c}}$ where g [nM/mm] indicates a gradient strength, a' is the estimated cell length, and $\bar{c}$ is an average concentration [33]. Typically, the gradient detection limit is considered in a simple spherical cell model with an estimated cell diameter a. Yet, migrating eKICs have mesenchymal morphology that displays extremely elongated shapes along with their movement direction. [19] For that reason, we assumed that the molecule variance across the cell body was enhanced by the mesenchymal morphology. In considering the morphology of eKICs, we defined the estimated cell length as $a' = a \times S$ and adjusted the ellipsoidal shape factor S. For simplicity, we assumed that the receptor distributed equally on the cells' surfaces in determining the shape factor S =1.69 and defined a ratio of the ellipsoid's surface area (~1:10 aspect ratio in measurement) to the sphere. As a result, we split the center channel regions into a) $\bar{p}$ > ~1% and b) $\bar{p}$ < ~1% based on the split line reaching the physical detection limit of the cells, which was assumed as ~1% (Figure 5.6). In other words, the cells in region b) of $\nabla T + v_f^+$ and region a) $\nabla T + v_f^-$ were exposed to the shallow gradient of TGF-β below the physical detection limit, implying that the cells might not sense the gradient.

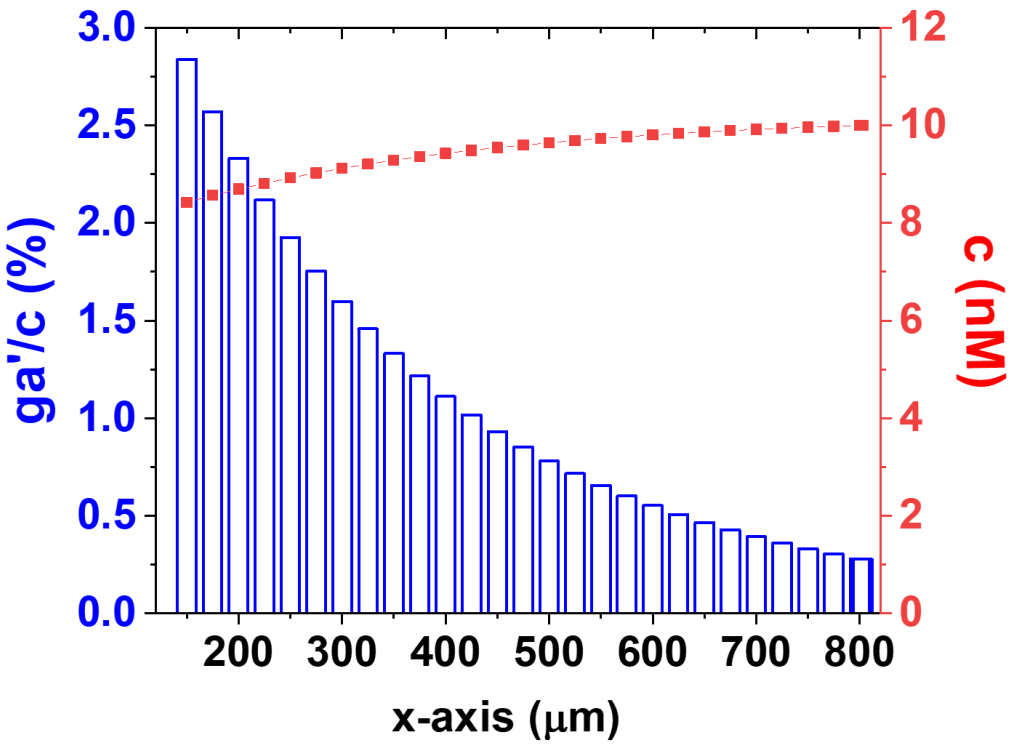

Figure 5.6. Estimated concentration change across the mesenchymal cell body, ga'/c (%) (blue) and concentration profiles c (nM) (red) along with x-axis (μm).

Although further research is needed to determine the true physical detection limit, by using a rough estimation for this limit, we assessed the cell migratory behaviors for the scenarios of ∇T + v_f^+ and ∇T + v_f^- (Figure 5.7A and B, respectively). For ∇T + v_f^+, the signal environment in region a) included the shallow TGF-β gradient, which was above but close to the physical detection limit. The flow signal was applied in the same direction to the TGF-β gradient, implying additive stimulations. Indeed, cell directional accuracy was highly enhanced in region a) of ∇T + v_f^+ with a median DAI = 0.625. By contrast, the directional accuracy of the cells in region b) was significantly suppressed. The median DAI in the distribution approached near 0, indicating random motion. Considering that the chemical gradient in region b) was too shallow for the cells to sense, the effect of the TGF-β gradient was thought to be negligible. The cells in b) were experiencing the flow signal with a higher concentration background of TGF-β. Interestingly, the bias effect that was induced by the flow signal was also eliminated, which suggests that the cell's innate capability in signal processing might constrain rheotaxis, which we hypothesized. The results imply that the

physical limit in the common processing of molecules of M* (see chapter 4) might be executed by flow signal processing as well.

The signal environment of $\nabla T + v_f -$ showed a similar distinction in two regions (as it did in $\nabla T + v_f^+$), except that the background concentration of TGF-β was considerably lower. Indeed, the cell behaviors in directional accuracy showed significant distinctions in two regions. Cells in region b) with the shallow gradient were biased toward the TGF-β gradient direction, even though the flow signal was applied in the opposite direction to the TGF-β gradient. The median of DAI distribution approached 0.531, implying that the chemotaxis might highly effective than the flow signal. Conversely, the cells in region a) seemed to show bias in the opposite direction of the TGF-β gradient, which corresponded to the flow signal stimulation. The median DAI was -0.163, indicating that the cell movements were slightly biased toward following the upstream flow direction, which demonstrated that stimulation of the TGF-β gradient was delineated. Although it showed slight bias accuracy toward the flow upstream, it is unclear in statistical analysis. Further research warrants in investigating the quantitative comparison of effectiveness between chemical and the flow signals.

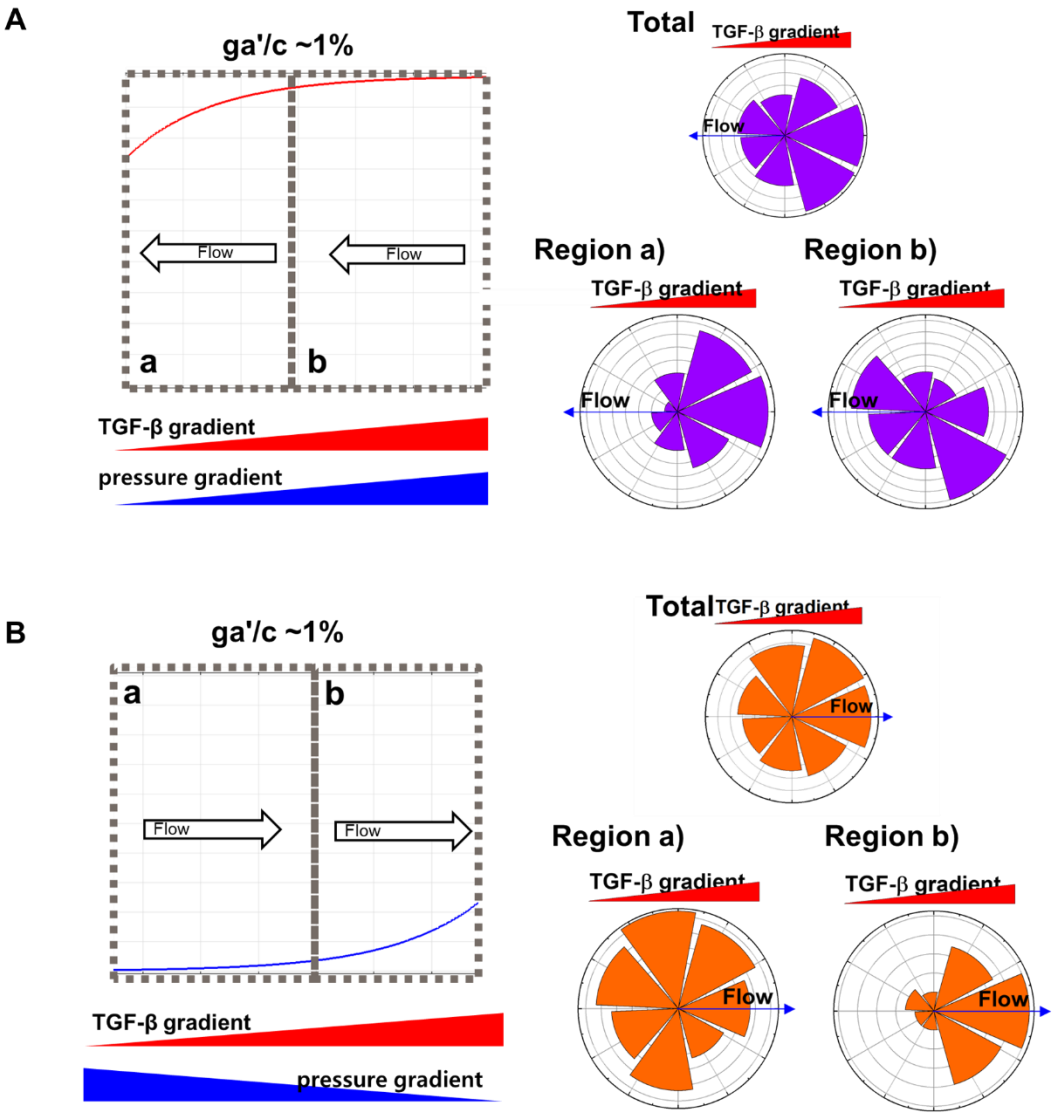

Figure 5.7. The directional angle (θ) distribution depending on the location where split by the physical detection limit of (A) $\nabla T+ V_f+$ (purple), and (B) $\nabla T+ V_f-$ (orange)

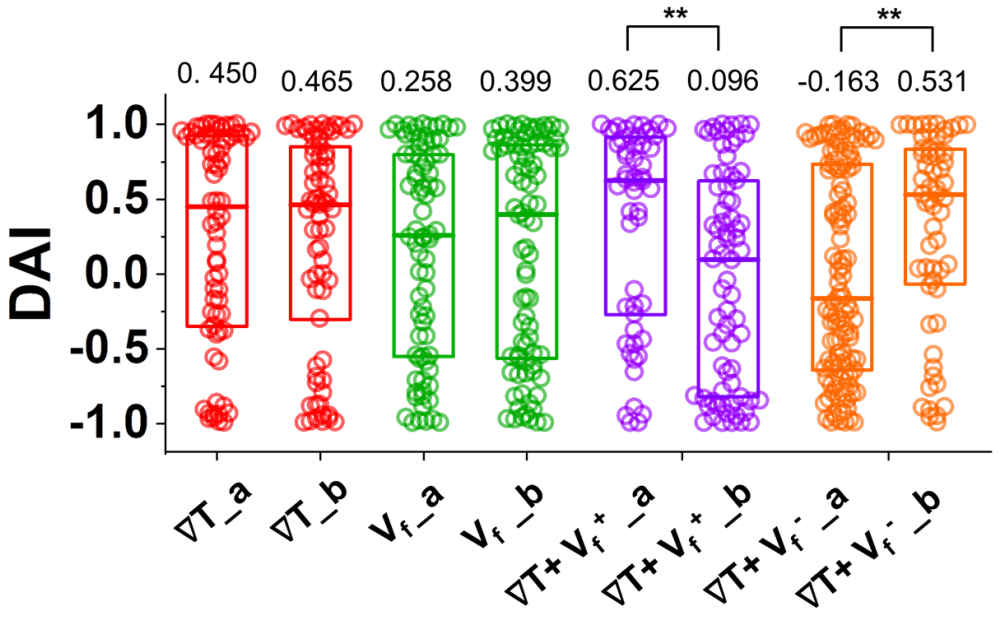

Figure 5.8. Directional accuracy index (DAI) distributions of all collected trajectories. ;n≥3. **: p<.01, (Mann-Whitney test). Dot; DAI from a single trajectory. Box: quartiles with a median line in the middle of the box.

5.4 Discussion

The present results elicit the cell migratory response to the combined signal environment of TGF-β combined with interstitial flow. We evaluated the effect of the complex signal environment by physically decoupling the signals. The flow-applied signal environment alters the TGF-β concentration profiles in non-linear exponentials, where the cells experience the shallow gradient close to the physical detection limit. The cells' movement was highly biased even with the shallow gradient but above the physical detection limit. The flow signal applied in the same direction to the TGF- β gradient seems to contribute to the bias accuracy of cells under the chemotactic response. In contrast, it does not compete with the TGF-β chemotaxis when they applied in the opposite direction. Interestingly, the directional accuracy of cell migration induced by the flow signal was ruled out when cells were exposed to the higher background concentration of TGF- β. Although it remains further research, it is thought that a cell capability in signal processing reaches the physical limit, implicating the chemotaxis and rheotaxis sharing the downstream transduction.

This study provides a novel insight for understanding the cellular process in directed migration based on physical and quantitative approaches using a controllable engineered microenvironment.

In this study, we described two scenarios in Pe~1- i) the flow direction is aligned to the TGF-β gradient, and ii) the flow direction is opposite to the TGF-β gradient. A valuable question can then be discussed: are these cases possibly applicable in actual tumor metastasis? The implication of our results in applying actual physiological conditions in the tumor is highly important. Recent studies reported that the heterogeneous features in the IFP variation are observed in the interstitial region depending on the cancer type and patient [127, 133]. Notably, increased IFP at the core of the solid tumor such as pancreatic adenocarcinoma (PDAC) profoundly impede the interstitial fluid flow getting perfused through the tumor tissue, whereas the periphery region IFP is significantly lower than the core [127, 147, 148]. It drives the aberrant interstitial flow. Meanwhile, cancer cells near peripheral boundaries of the solid tumor abut the dense stroma, which upregulates the chemical signals such as TGF-β. The physiological condition is highly corresponding to our second scenario. The present results showed that significant biased features in the cell migration even under the shallow gradient close to the physical detection limit, implying tumor cells near the peripheral encounter the signal environment that may increase the metastatic potential (Figure 5.9). Indeed, cell dissemination of the primary tumors was observed *in vivo* at the peripheral region [41].

Although we considered the effect of the complex signal environment by decoupling those in a physical approach, further advances can help to prove the concept by elucidating explicit molecular study. Specifically, it is largely unknown how cells sense and process the flow as a mechanical signal. The approach can be strengthened by further research of potential intracellular signaling molecules activated by the flow signals. Moreover, the actual physiological condition is barely available due to its heterogeneity and difficulties in measurement. Many recent studies highlighted the importance of the interstitial flow in the tumor microenvironment. [127, 133, 148] The study from Hompland., et al, showed the peritumoral flow rate is closely relative to the patient's survival rate [133]. In this sense, the measuring technique for the physiological conditions will contribute to advancing the understanding of the effect of the flow signals in the complex signal environment, which will help establishing a novel therapeutic strategy of a controlled signal environment.

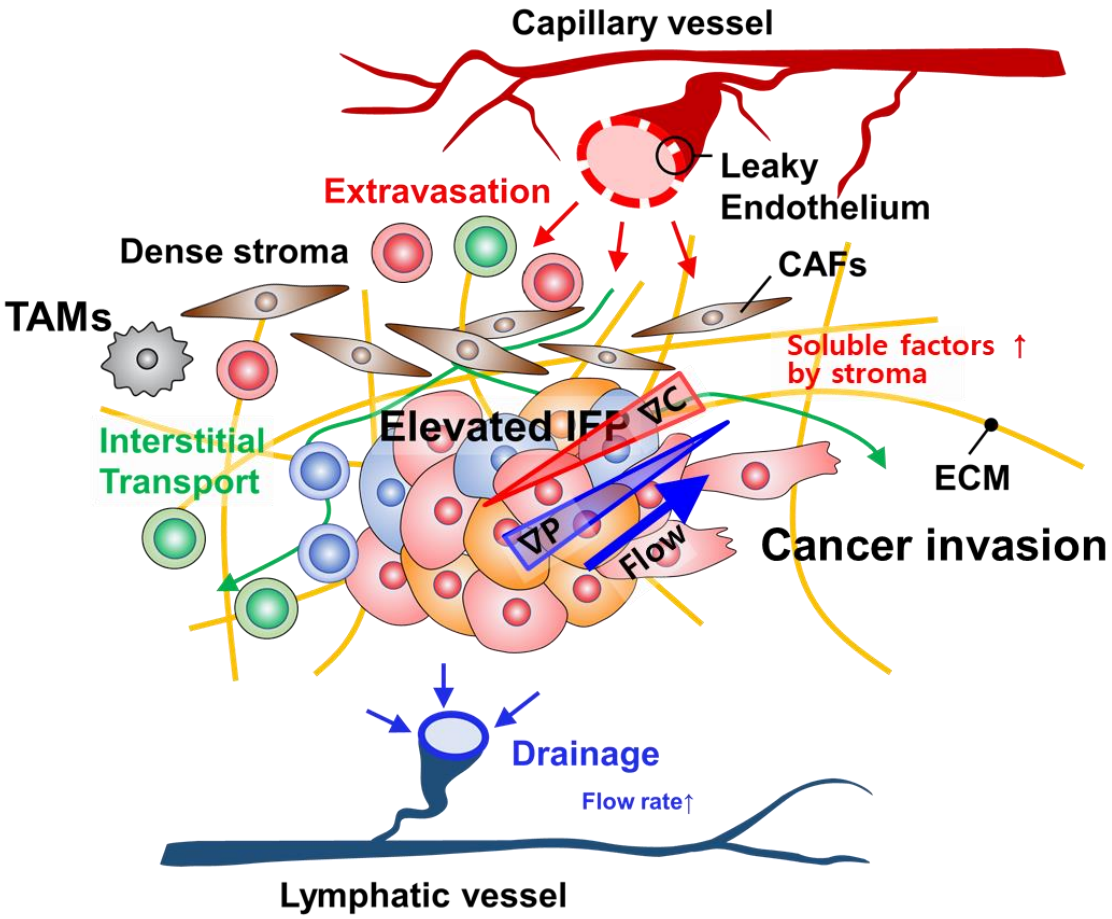

Figure 5.9. Schematic of distinct features in the tumor microenvironment

APPENDIX A. SYMMETRY TEST FOR DIRECTIONAL ANGLE DISTRIBUTION

Throughout the study, the directional accuracy was evaluated to illustrate the directional performance of directed cell migration. The directional accuracy was denoted as a directional accuracy index (DAI) or chemotactic index (CI) defined with cosine function of angle (θ) between cell displacement and environmental cue directions:

$$DAI = CI = cos\theta$$

As noted in chapter 3, the directional accuracy indicated how the cell movement accurately follow the environmental cue direction. In other words, the DAI (or CI) is a metric to assess the directional performance along with the specific direction. It cannot represent the directional performance of the trajectories toward the other directions. To verify the environmental stimulations (a TGF-β gradient or combined signal environment driven by convection) does not significantly influence the directional performance toward the other directions, we investigated the symmetry in the angle (θ) distribution of eKIC trajectories in control, a TGF-β gradient (∇T), TGF-β gradient with + flow (∇T+ V_f+), and TGF-β gradient with - flow (∇T+ Vf -). Details for each experimental control was illustrated in chapter 5.

In the angle distribution as shown in the Figure A.1, we defined x-axis as a direction of the environmental cues. Initially, we assessed the x-axis symmetry by considering the sign of the angles. x-axis symmetry indicates that the cell movement is not biased toward the perpendicular direction of the environmental cues, where the cells do not contain any constraint or stimulation. In comparison of the distributions between θ and -θ, the symmetry can be confirmed when they have not significant differences, whereas the statistically significant difference indicates that the x-axis symmetry is ruled out in the distribution. For the comparison, we assessed Kolmogorov-Smirnov test. In results, all of the experimental conditions showed $p>0.05$ as indicated in Figure A.2.

.

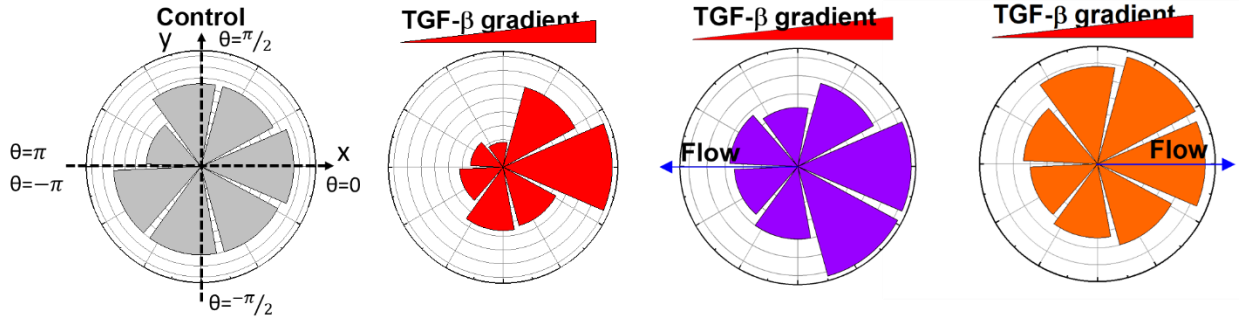

Figure A.1. Polar distribution of directional angles (θ) of eKIC trajectories in control (Ctrl, grey), 10nM/mm of TGF-β gradient (∇T, red), 10nM/mm of TGF-β gradient with 1μm/s of the flow from the source to sink channels (∇T+ Vf+, purple), and 10nM/mm of TGF-β gradient with 1μm/s of the flow from the sink to source channels (∇T+ Vf -, orange). N_t (trajectories) >100 for each experimental group from n≥3. Plot: (r,θ) where r indicates the number of trajectories which is normalized.

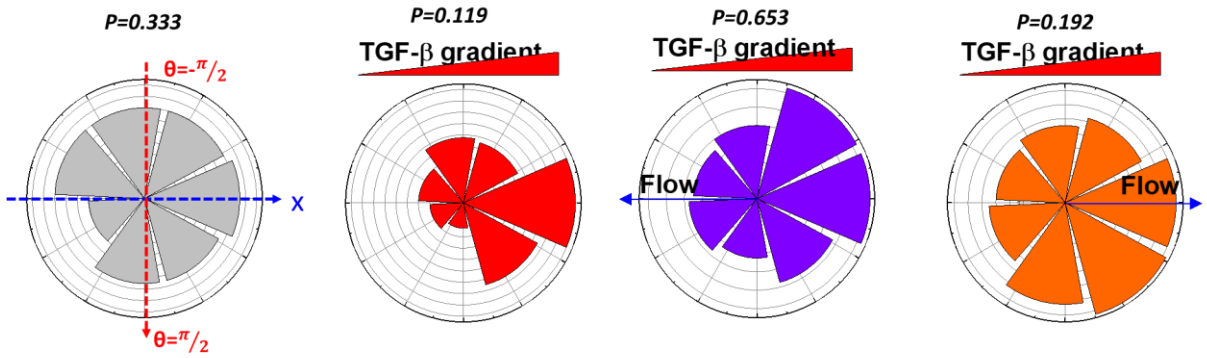

Figure A.2. x-axis symmetry. Polar distribution of negative directional angles (-θ) of eKIC trajectories in Ctrl (grey) ∇T (red), ∇T+ Vf+ (purple), and ∇T+ Vf – (orange). Kolmogorov-Smirnov test was assessed with raw distribution between θ and -θ with p<.05.

Next, we assessed the symmetry test along with y-axis. Since the environmental cue direction is aligned to x-axis, the y-axis symmetry is crucially relevant the cell response to the environmental stimuli. In assessing the y-axis symmetry, the angle was transmitted to $\theta' = \theta - \frac{\pi}{2}$. And the distribution change between θ' and - θ' was statistically analyzed as it did for x-axis symmetry. In results shown in Figure A.3, the directional angle of eKIC trajectories in ∇T only showed the statistically significant change ($p << 0.001$), indicating the symmetry was suspended whereas all

the other cases still showed the y-axis symmetry. The results are corresponding the DAI evaluation in chapter 5.

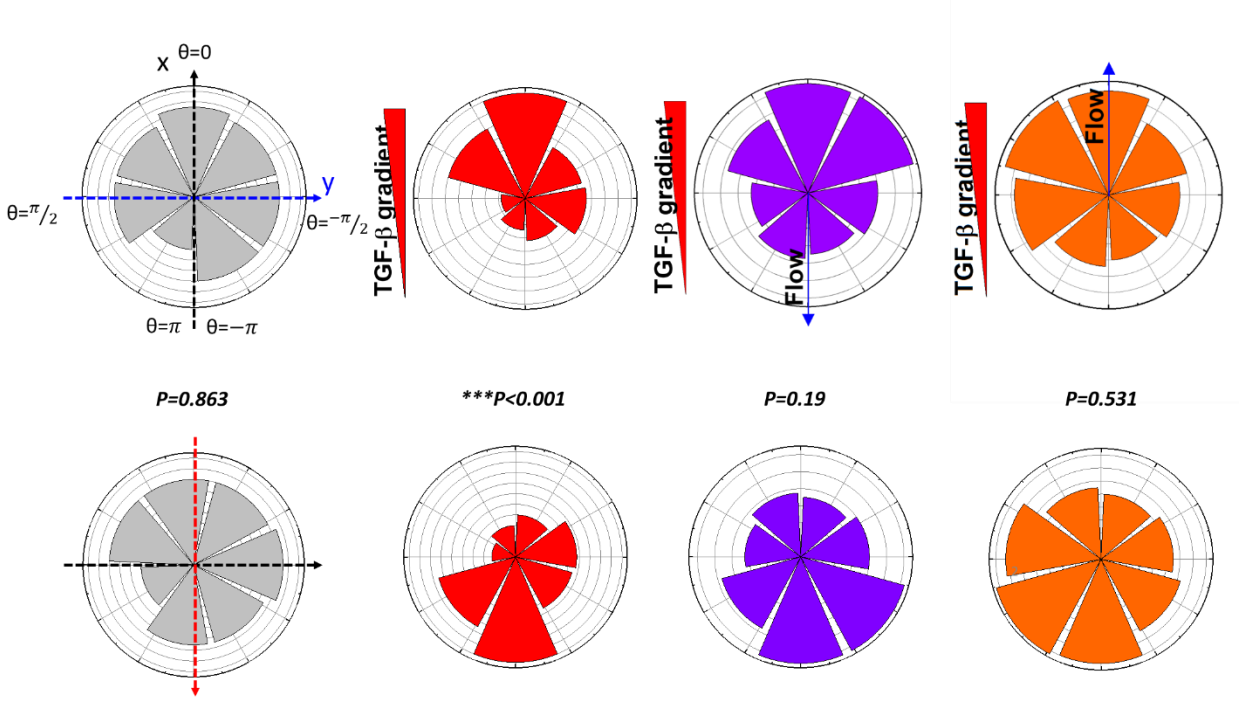

Figure A.3. y-axis symmetry. Polar distribution of directional angles θ' (θ-$\frac{\pi}{2}$, upper) and – θ' (bottom) of eKIC trajectories in Ctrl (grey) ∇T (red), ∇T+ Vf+ (purple), and ∇T+ Vf – (orange). Kolmogorov-Smirnov test was assessed with raw distribution between θ' and -θ' : ***p<<.001.

REFERENCES

1. McSherry, E.A., et al., *Common Molecular Mechanisms of Mammary Gland Development and Breast Cancer.* Cellular and Molecular Life Sciences, 2007. **64**(24): p. 3201-3218.
2. Weijer, C.J., *Collective cell migration in development.* Journal of Cell Science, 2009. **122**(18): p. 3215-3223.
3. Bischoff, R., *Chemotaxis of skeletal muscle satellite cells.* Developmental dynamics, 1997. **208**(4): p. 505-515.
4. Roussos, E.T., J.S. Condeelis, and A. Patsialou, *Chemotaxis in cancer.* Nature Reviews Cancer, 2011. **11**(8): p. 573-587.
5. Beltman, J.B., A.F.M. Marée, and R.J.d. Boer, *Analysing immune cell migration.* Nature Reviews Immunology, 2009. **9**(11): p. 789-798.
6. Horwitz, A.R. and J.T. Parsons, *Cell Migration--Movin' On.* Science, 1999. **286**(5442): p. 1102-1103.
7. Vicente-Manzanares, M., *Cell migration at a glance.* Journal of Cell Science, 2005. **118**(21): p. 4917-4919.
8. Nguyen, D.X., P.D. Bos, and J. Massagué, *Metastasis: from dissemination to organ-specific colonization.* Nature Reviews Cancer, 2009. **9**(4): p. 274-284.
9. Woodhouse, E.C., R.F. Chuaqui, and L.A. Liotta, *General mechanisms of metastasis.* Cancer, 1997. **80**(S8): p. 1529-1537.
10. Odenthal, J., R. Takes, and P. Friedl, *Plasticity of tumor cell invasion: governance by growth factors and cytokines.* Carcinogenesis, 2016. **37**(12): p. 1117-1128.
11. Ozcelikkale, A., et al., *In vitro microfluidic models of tumor microenvironment to screen transport of drugs and nanoparticles.* Wiley Interdisciplinary Reviews: Nanomedicine and Nanobiotechnology, 2017. **9**(5): p. e1460.
12. Popović, M., et al., *Active dynamics of tissue shear flow.* New Journal of Physics, 2017. **19**(3): p. 033006.
13. Swartz, M.A. and M.E. Fleury, *Interstitial Flow and Its Effects in Soft Tissues.* Annual Review of Biomedical Engineering, 2007. **9**(1): p. 229-256.
14. Polacheck, W.J., I.K. Zervantonakis, and R.D. Kamm, *Tumor cell migration in complex microenvironments.* Cellular and Molecular Life Sciences, 2013. **70**(8): p. 1335-1356.
15. Griffith, L.G. and M.A. Swartz, *Capturing complex 3D tissue physiology in vitro.* Nature Reviews Molecular Cell Biology, 2006. **7**(3): p. 211-224.
16. Truong, D., et al., *Breast Cancer Cell Invasion into a Three Dimensional Tumor-Stroma Microenvironment.* Scientific Reports, 2016. **6**(1).
17. Paul, C.D., P. Mistriotis, and K. Konstantopoulos, *Cancer cell motility: lessons from migration in confined spaces.* Nature Reviews Cancer, 2016. **17**(2): p. 131-140.
18. Friedl, P. and S. Alexander, *Cancer invasion and the microenvironment: plasticity and reciprocity.* Cell, 2011. **147**(5): p. 992-1009.
19. Clark, A.G. and D.M. Vignjevic, *Modes of cancer cell invasion and the role of the microenvironment.* Current Opinion in Cell Biology, 2015. **36**: p. 13-22.
20. Oudin, M.J. and V.M. Weaver, *Physical and Chemical Gradients in the Tumor Microenvironment Regulate Tumor Cell Invasion, Migration, and Metastasis.* Cold Spring Harbor Symposia on Quantitative Biology, 2017: p. 030817.

21. Charras, G. and E. Sahai, *Physical influences of the extracellular environment on cell migration.* Nature Reviews Molecular Cell Biology, 2014. **15**(12): p. 813-824.
22. Mak, M., et al., *Single-Cell Migration in Complex Microenvironments: Mechanics and Signaling Dynamics.* Journal of Biomechanical Engineering, 2016. **138**(2): p. 021004.
23. Baker, B.M. and C.S. Chen, *Deconstructing the third dimension – how 3D culture microenvironments alter cellular cues.* J Cell Sci, 2012. **125**(13): p. 3015-3024.
24. Quail, D.F. and J.A. Joyce, *Microenvironmental regulation of tumor progression and metastasis.* Nature Medicine, 2013. **19**(11): p. 1423-1437.
25. Ellison, D., et al., *Cell–cell communication enhances the capacity of cell ensembles to sense shallow gradients during morphogenesis.* Proceedings of the National Academy of Sciences, 2016. **113**(6): p. E679-E688.
26. Wang, S.-J., et al., *Differential effects of EGF gradient profiles on MDA-MB-231 breast cancer cell chemotaxis.* Experimental cell research, 2004. **300**(1): p. 180-189.
27. Sidani, M., et al., *Cofilin determines the migration behavior and turning frequency of metastatic cancer cells.* The Journal of Cell Biology, 2007. **179**(4): p. 777-791.
28. Bravo-Cordero, J.J., et al., *Functions of cofilin in cell locomotion and invasion.* Nature Reviews Molecular Cell Biology, 2013. **14**: p. 405.
29. Polacheck, W.J., J.L. Charest, and R.D. Kamm, *Interstitial flow influences direction of tumor cell migration through competing mechanisms.* Proceedings of the National Academy of Sciences, 2011. **108**(27): p. 11115-11120.
30. Uttamsingh, S., et al., *Synergistic effect between EGF and TGF-β1 in inducing oncogenic properties of intestinal epithelial cells.* Oncogene, 2008. **27**(18): p. 2626-2634.
31. Endres, R.G. and N.S. Wingreen, *Accuracy of direct gradient sensing by single cells.* Proceedings of the National Academy of Sciences, 2008. **105**(41): p. 15749-15754.
32. Hughes-Alford, S.K. and D.A. Lauffenburger, *Quantitative analysis of gradient sensing: towards building predictive models of chemotaxis in cancer.* Current Opinion in Cell Biology, 2012. **24**(2): p. 284-291.
33. Varennes, J. and A. Mugler, *Sense and sensitivity: physical limits to multicellular sensing, migration and drug response.* Molecular Pharmaceutics, 2016.
34. Van Haastert, P.J.M. and P.N. Devreotes, *Chemotaxis: signalling the way forward.* Nature Reviews Molecular Cell Biology, 2004. **5**(8): p. 626-634.
35. Starbuck, C. and D.A. Lauffenburger, *Mathematical model for the effects of epidermal growth factor receptor trafficking dynamics on fibroblast proliferation responses.* Biotechnology Progress, 1992. **8**(2): p. 132-143.
36. Harley, B.A.C., et al., *Microarchitecture of Three-Dimensional Scaffolds Influences Cell Migration Behavior via Junction Interactions.* Biophysical Journal, 2008. **95**(8): p. 4013-4024.
37. Petrie, R.J. and K.M. Yamada, *Multiple mechanisms of 3D migration: the origins of plasticity.* Current Opinion in Cell Biology, 2016. **42**: p. 7-12.
38. Trepat, X., et al., *Physical forces during collective cell migration.* Nature Physics, 2009. **5**: p. 426.
39. Wolf, K., et al., *Physical limits of cell migration: Control by ECM space and nuclear deformation and tuning by proteolysis and traction force.* The Journal of Cell Biology, 2013. **201**(7): p. 1069-1084.
40. Ladoux, B. and A. Nicolas, *Physically based principles of cell adhesion mechanosensitivity in tissues.* Reports on Progress in Physics, 2012. **75**(11): p. 116601.

41. Wirtz, D., K. Konstantopoulos, and P.C. Searson, *The physics of cancer: the role of physical interactions and mechanical forces in metastasis.* Nature Reviews Cancer, 2011. **11**(7): p. 512-522.
42. Veltman, D.M., I. Keizer-Gunnik, and P.J.M.V. Haastert, *Four key signaling pathways mediating chemotaxis in Dictyostelium discoideum.* J Cell Biol, 2008. **180**(4): p. 747-753.
43. Goldstein, B. and M. Dembo, *Approximating the effects of diffusion on reversible reactions at the cell surface: ligand-receptor kinetics.* Biophysical Journal, 1995. **68**(4): p. 1222-1230.
44. Van Haastert, P.J.M. and M. Postma, *Biased random walk by stochastic fluctuations of chemoattractant-receptor interactions at the lower limit of detection.* Biophysical journal, 2007. **93**(5): p. 1787-1796.
45. Kraning-Rush, C.M., et al., *The role of the cytoskeleton in cellular force generation in 2D and 3D environments.* Physical Biology, 2011. **8**(1): p. 015009.
46. Affolter, M. and C.J. Weijer, *Signaling to Cytoskeletal Dynamics during Chemotaxis.* Developmental Cell, 2005. **9**(1): p. 19-34.
47. Masuda, H., et al., *Role of epidermal growth factor receptor in breast cancer.* Breast Cancer Research and Treatment, 2012. **136**(2): p. 331-345.
48. Dang, I., et al., *Inhibitory signalling to the Arp2/3 complex steers cell migration.* Nature, 2013. **503**(7475): p. 281-284.
49. Brayford, S., et al., *The Role of the Actin Cytoskeleton in Cancer and Its Potential Use as a Therapeutic Target*, in *The Cytoskeleton in Health and Disease*. 2015, Springer, New York, NY. p. 373-391.
50. Lee, J.J.X., K. Loh, and Y.-S. Yap, *PI3K/Akt/mTOR inhibitors in breast cancer.* Cancer Biology & Medicine, 2015. **12**(4): p. 342-354.
51. Bosgraaf, L., I. Keizer-Gunnink, and P.J.M. Van Haastert, *PI3-kinase signaling contributes to orientation in shallow gradients and enhances speed in steep chemoattractant gradients.* Journal of Cell Science, 2008. **121**(21): p. 3589-3597.
52. Funamoto, S., et al., *Role of Phosphatidylinositol 3 Kinase and a Downstream Pleckstrin Homology Domain–Containing Protein in Controlling Chemotaxis inDictyostelium.* The Journal of cell biology, 2001. **153**(4): p. 795-810.
53. Paul, C.D., P. Mistriotis, and K. Konstantopoulos, *Cancer cell motility: lessons from migration in confined spaces.* Nature Reviews Cancer, 2017. **17**(2): p. 131.
54. Um, E., et al., *Cell migration in microengineered tumor environments.* Lab on a Chip, 2017. **17**(24): p. 4171-4185.
55. Lemmon, M.A. and J. Schlessinger, *Cell Signaling by Receptor Tyrosine Kinases.* Cell, 2010. **141**(7): p. 1117-1134.
56. Hood, J.D. and D.A. Cheresh, *Role of integrins in cell invasion and migration.* Nature Reviews Cancer, 2002. **2**(2): p. 91-100.
57. Rudzka, D.A. and M.F. Olson, *Microtrack migration: insights into 3D cell motility. Focus on "Comparative mechanisms of cancer cell migration through 3D matrix and physiological microtracks".* American Journal of Physiology-Cell Physiology, 2015. **308**(6): p. C434-C435.
58. Truskey, G.A., F. Yuan, and D.F. Katz, *Transport phenomena in biological systems.* 2004.
59. Codling, E.A., M.J. Plank, and S. Benhamou, *Random walk models in biology.* Journal of the Royal Society Interface, 2008. **5**(25): p. 813-834.

60. Gorelik, R. and A. Gautreau, *Quantitative and unbiased analysis of directional persistence in cell migration.* Nature protocols, 2014. **9**(8): p. 1931-1943.
61. Petrie, R.J., A.D. Doyle, and K.M. Yamada, *Random versus directionally persistent cell migration.* Nature Reviews Molecular Cell Biology, 2009. **10**(8): p. 538-549.
62. Patlak, C.S., *Random walk with persistence and external bias.* Bulletin of Mathematical Biology, 1953. **15**(3): p. 311-338.
63. Boyden, S., *The chemotactic effect of mixtures of antibody and antigen on polymorphonuclear leucocytes.* Journal of Experimental Medicine, 1962. **115**(3): p. 453-466.
64. Keizer-Gunnink, I., A. Kortholt, and P.J.M.V. Haastert, *Chemoattractants and chemorepellents act by inducing opposite polarity in phospholipase C and PI3-kinase signaling.* The Journal of Cell Biology, 2007. **177**(4): p. 579-585.
65. Prentice-Mott, H.V., et al., *Directional memory arises from long-lived cytoskeletal asymmetries in polarized chemotactic cells.* Proceedings of the National Academy of Sciences, 2016. **113**(5): p. 1267-1272.
66. Woodham, E.F. and L.M. Machesky, *Polarised cell migration: intrinsic and extrinsic drivers.* Current Opinion in Cell Biology, 2014. **30**: p. 25-32.
67. Dou, J. and J.-M. Lin, *Cell Migration with Microfluidic Chips*, in *Cell Analysis on Microfluidics*. 2018, Springer, Singapore. p. 149-179.
68. Atencia, J. and D.J. Beebe. *Controlled microfluidic interfaces*. Nature [Special Features] 2004.
69. Atencia, J., J. Morrow, and L. E. Locascio, *The microfluidic palette: A diffusive gradient generator with spatio-temporal control.* Lab on a Chip, 2009. **9**(18): p. 2707-2714.
70. Huang, Y., et al., *Microfluidics-based devices: New tools for studying cancer and cancer stem cell migration.* Biomicrofluidics, 2011. **5**(1): p. 013412.
71. Lin, B. and A. Levchenko, *Spatial Manipulation with Microfluidics.* Frontiers in Bioengineering and Biotechnology, 2015. **3**(39).
72. Aizel, K., et al., *A tuneable microfluidic system for long duration chemotaxis experiments in a 3D collagen matrix.* Lab on a Chip, 2017. **17**(22): p. 3851-3861.
73. Wang, X., Z. Liu, and Y. Pang, *Concentration gradient generation methods based on microfluidic systems.* RSC Advances, 2017. **7**(48): p. 29966-29984.
74. Haessler, U., et al., *Dendritic cell chemotaxis in 3D under defined chemokine gradients reveals differential response to ligands CCL21 and CCL19.* Proceedings of the National Academy of Sciences, 2011. **108**(14): p. 5614-5619.
75. Jacquemet, G., H. Hamidi, and J. Ivaska, *Filopodia in cell adhesion, 3D migration and cancer cell invasion.* Current Opinion in Cell Biology, 2015. **36**: p. 23-31.
76. Driscoll, M.K. and G. Danuser, *Quantifying Modes of 3D Cell Migration.* Trends in Cell Biology, 2015. **25**(12): p. 749-759.
77. Iglesias, P.A. and P.N. Devreotes, *Navigating through models of chemotaxis.* Current opinion in cell biology, 2008. **20**(1): p. 35-40.
78. Kim, B.J., et al., *Cooperative roles of SDF-1α and EGF gradients on tumor cell migration revealed by a robust 3D microfluidic model.* PloS one, 2013. **8**(7): p. e68422.
79. Shields, J.D., et al., *Autologous chemotaxis as a mechanism of tumor cell homing to lymphatics via interstitial flow and autocrine CCR7 signaling.* Cancer cell, 2007. **11**(6): p. 526-538.

80. Witsch, E., M. Sela, and Y. Yarden, *Roles for Growth Factors in Cancer Progression.* Physiology, 2010. **25**(2): p. 85-101.
81. Kay, R.R., et al., *Changing directions in the study of chemotaxis.* Nature Reviews Molecular Cell Biology, 2008. **9**(6): p. 455-463.
82. Mouneimne, G., et al., *Spatial and temporal control of cofilin activity is required for directional sensing during chemotaxis.* Current biology, 2006. **16**(22): p. 2193-2205.
83. Nelson, R.D., P.G. Quie, and R.L. Simmons, *Chemotaxis under agarose: a new and simple method for measuring chemotaxis and spontaneous migration of human polymorphonuclear leukocytes and monocytes.* The Journal of Immunology, 1975. **115**(6): p. 1650-1656.
84. Fiedler, J., et al., *VEGF-A and PlGF-1 stimulate chemotactic migration of human mesenchymal progenitor cells.* Biochemical and biophysical research communications, 2005. **334**(2): p. 561-568.
85. Iellem, A., et al., *Unique chemotactic response profile and specific expression of chemokine receptors CCR4 and CCR8 by CD4+ CD25+ regulatory T cells.* The Journal of experimental medicine, 2001. **194**(6): p. 847-854.
86. Mayr-Wohlfart, U., et al., *Vascular endothelial growth factor stimulates chemotactic migration of primary human osteoblasts.* Bone, 2002. **30**(3): p. 472-477.
87. McCutcheon, M., *Chemotaxis in leukocytes.* Physiological reviews, 1946. **26**(3): p. 319-336.
88. Varennes, J., et al., *Emergent versus individual-based multicellular chemotaxis.* Physical review letters, 2017. **119**(18): p. 188101.
89. Giampieri, S., et al., *Localized and reversible TGFβ signalling switches breast cancer cells from cohesive to single cell motility.* Nature Cell Biology, 2009. **11**(11): p. 1287-1296.
90. Ikushima, H. and K. Miyazono, *TGFβ signalling: a complex web in cancer progression.* Nature Reviews Cancer, 2010. **10**(6): p. 415-424.
91. Kleuser, B., et al., *17-β-Estradiol Inhibits Transforming Growth Factor-β Signaling and Function in Breast Cancer Cells via Activation of Extracellular Signal-Regulated Kinase through the G Protein-Coupled Receptor 30.* Molecular Pharmacology, 2008. **74**(6): p. 1533-1543.
92. Luwor, R.B., et al., *Single live cell TGF-β signalling imaging: breast cancer cell motility and migration is driven by sub-populations of cells with dynamic TGF-β-Smad3 activity.* Molecular Cancer, 2015. **14**: p. 50.
93. Venturoli, D. and B. Rippe, *Ficoll and dextran vs. globular proteins as probes for testing glomerular permselectivity: effects of molecular size, shape, charge, and deformability.* American Journal of Physiology-Renal Physiology, 2005. **288**(4): p. F605-F613.
94. Varennes, J., et al., *Physical constraints on accuracy and persistence during breast cancer cell chemotaxis.* PLOS Computational Biology, 2019. **15**(4): p. e1006961.
95. Graner, F. and J.A. Glazier, *Simulation of biological cell sorting using a two-dimensional extended Potts model.* Physical review letters, 1992. **69**(13): p. 2013.
96. Swat, M.H., et al., *Multi-scale modeling of tissues using CompuCell3D.* Methods in cell biology, 2012. **110**: p. 325.
97. Szabó, A., et al., *Collective cell motion in endothelial monolayers.* Physical biology, 2010. **7**(4): p. 046007.
98. Varennes, J., B. Han, and A. Mugler, *Collective chemotaxis through noisy multicellular gradient sensing.* Biophysical Journal, 2016. **111**(3): p. 640-649.

99. Alt, W., *Biased random walk models for chemotaxis and related diffusion approximations.* Journal of mathematical biology, 1980. **9**(2): p. 147-177.
100. Othmer, H.G., S.R. Dunbar, and W. Alt, *Models of dispersal in biological systems.* Journal of mathematical biology, 1988. **26**(3): p. 263-298.
101. Fraley, S.I., et al., *Dimensional and temporal controls of three-dimensional cell migration by zyxin and binding partners.* Nature Communications, 2012. **3**: p. 719.
102. Mugler, A., A. Levchenko, and I. Nemenman, *Limits to the precision of gradient sensing with spatial communication and temporal integration.* Proceedings of the National Academy of Sciences, 2016. **113**(6): p. E689.
103. Swaney, K.F., C.-H. Huang, and P.N. Devreotes, *Eukaryotic Chemotaxis: A Network of Signaling Pathways Controls Motility, Directional Sensing, and Polarity.* Annual Review of Biophysics, 2010. **39**(1): p. 265-289.
104. Charest, P.G. and R.A. Firtel, *Big roles for small GTPases in the control of directed cell movement.* Biochemical Journal, 2007. **401**(2): p. 377-390.
105. Chung, C.Y., S. Funamoto, and R.A. Firtel, *Signaling pathways controlling cell polarity and chemotaxis.* Trends in biochemical sciences, 2001. **26**(9): p. 557-566.
106. Hart, S., et al., *GPCR-induced migration of breast carcinoma cells depends on both EGFR signal transactivation and EGFR-independent pathways.* Biological chemistry, 2005. **386**(9): p. 845-855.
107. Lappano, R. and M. Maggiolini, *G protein-coupled receptors: novel targets for drug discovery in cancer.* Nature reviews Drug discovery, 2011. **10**(1): p. 47-60.
108. Shi, Q. and Y.-G. Chen, *Interplay between TGF-β signaling and receptor tyrosine kinases in tumor development.* Science China Life Sciences, 2017. **60**(10): p. 1133-1141.
109. Wang, S.-J., et al., *Differential effects of EGF gradient profiles on MDA-MB-231 breast cancer cell chemotaxis.* Experimental Cell Research, 2004. **300**(1): p. 180-189.
110. Biswenger, V., et al., *Characterization of EGF-guided MDA-MB-231 cell chemotaxis in vitro using a physiological and highly sensitive assay system.* PloS one, 2018. **13**(9).
111. Fernandis, A.Z., et al., *Regulation of CXCR4-mediated chemotaxis and chemoinvasion of breast cancer cells.* Oncogene, 2004. **23**(1): p. 157-167.
112. Koshiba, T., et al., *Expression of stromal cell-derived factor 1 and CXCR4 ligand receptor system in pancreatic cancer: a possible role for tumor progression.* Clinical cancer research, 2000. **6**(9): p. 3530-3535.
113. Mosadegh, B., et al., *Epidermal growth factor promotes breast cancer cell chemotaxis in CXCL12 gradients.* Biotechnology and bioengineering, 2008. **100**(6): p. 1205-1213.
114. Gore, J., et al., *Combined targeting of TGF-β, EGFR and HER2 suppresses lymphangiogenesis and metastasis in a pancreatic cancer model.* Cancer Letters, 2016. **379**(1): p. 143-153.
115. Pang, M., et al., *TGF-β1-induced EMT promotes targeted migration of breast cancer cells through the lymphatic system by the activation of CCR7/CCL21-mediated chemotaxis.* Oncogene, 2016. **35**(6): p. 748-760.
116. Han, W. and H.-W. Lo, *Landscape of EGFR signaling network in human cancers: biology and therapeutic response in relation to receptor subcellular locations.* Cancer letters, 2012. **318**(2): p. 124-134.
117. Sempere, L.F., J.R. Gunn, and M. Korc, *A novel 3-dimensional culture system uncovers growth stimulatory actions by TGFβ in pancreatic cancer cells.* Cancer Biology & Therapy, 2011. **12**(3): p. 198-207.

118. Whipple, C.A., A.L. Young, and M. Korc, *A KrasG12D-driven genetic mouse model of pancreatic cancer requires glypican-1 for efficient proliferation and angiogenesis.* Oncogene, 2011. **31**: p. 2535.
119. Harley, B.A., et al., *Microarchitecture of three-dimensional scaffolds influences cell migration behavior via junction interactions.* Biophysical journal, 2008. **95**(8): p. 4013-4024.
120. Chavez, K.J., S.V. Garimella, and S. Lipkowitz, *Triple negative breast cancer cell lines: One tool in the search for better treatment of triple negative breast cancer.* Breast Dis, 2010. **32**: p. 35-48.
121. Valastyan, S. and Robert A. Weinberg, *Tumor Metastasis: Molecular Insights and Evolving Paradigms.* Cell, 2011. **147**(2): p. 275-292.
122. Seeley, E.S., et al., *Pancreatic cancer and precursor pancreatic intraepithelial neoplasia lesions are devoid of primary cilia.* Cancer research, 2009. **69**(2): p. 422-430.
123. Bradney, M.J., et al., *A Biomimetic Tumor Model of Heterogeneous Invasion in Pancreatic Ductal Adenocarcinoma.* Small, 2020: p. 1905500.
124. Muller, P.A., K.H. Vousden, and J.C. Norman, *p53 and its mutants in tumor cell migration and invasion.* Journal of Cell Biology, 2011. **192**(2): p. 209-218.
125. Follain, G., et al., *Fluids and their mechanics in tumour transit: Shaping metastasis.* Nature Reviews Cancer, 2019: p. 1-18.
126. Swartz, M.A. and A.W. Lund, *Lymphatic and interstitial flow in the tumour microenvironment: linking mechanobiology with immunity.* Nature Reviews Cancer, 2012. **12**(3): p. 210-219.
127. Munson, J.M. and A.C. Shieh, *Interstitial fluid flow in cancer: implications for disease progression and treatment.* Cancer management and research, 2014. **6**: p. 317.
128. Mantovani, A., et al., *Macrophage polarization: tumor-associated macrophages as a paradigm for polarized M2 mononuclear phagocytes.* Trends in immunology, 2002. **23**(11): p. 549-555.
129. Ren, B., et al., *Tumor microenvironment participates in metastasis of pancreatic cancer.* Molecular Cancer, 2018. **17**(1): p. 108.
130. Jain, R.K., J.D. Martin, and T. Stylianopoulos, *The role of mechanical forces in tumor growth and therapy.* Annual review of biomedical engineering, 2014. **16**: p. 321-346.
131. Provenzano, Paolo P., et al., *Enzymatic Targeting of the Stroma Ablates Physical Barriers to Treatment of Pancreatic Ductal Adenocarcinoma.* Cancer Cell, 2012. **21**(3): p. 418-429.
132. Milosevic, M., et al., *Interstitial permeability and elasticity in human cervix cancer.* Microvascular research, 2008. **75**(3): p. 381-390.
133. Hompland, T., et al., *Peritumoral interstitial fluid flow velocity predicts survival in cervical carcinoma.* Radiotherapy and Oncology, 2014. **113**(1): p. 132-138.
134. Munson, J.M. and A.C. Shieh, *Interstitial fluid flow in cancer: implications for disease progression and treatment.* Cancer management and research, 2014. **6**: p. 317-328.
135. Dewhirst, M.W. and T.W. Secomb, *Transport of drugs from blood vessels to tumour tissue.* Nature Reviews Cancer, 2017. **17**(12): p. 738-750.
136. Prat, A., et al., *Characterization of cell lines derived from breast cancers and normal mammary tissues for the study of the intrinsic molecular subtypes.* Breast Cancer Research and Treatment, 2013. **142**(2): p. 237-255.

137. Galie, P.A. and J.P. Stegemann, *Simultaneous application of interstitial flow and cyclic mechanical strain to a three-dimensional cell-seeded hydrogel.* Tissue Engineering Part C: Methods, 2011. **17**(5): p. 527-536.
138. Polacheck, W.J., et al., *Mechanotransduction of fluid stresses governs 3D cell migration.* Proceedings of the National Academy of Sciences, 2014. **111**(7): p. 2447-2452.
139. Artemenko, Y., et al., *Chemical and mechanical stimuli act on common signal transduction and cytoskeletal networks.* Proceedings of the National Academy of Sciences, 2016. **113**(47): p. E7500-E7509.
140. Bradney, M.J., et al., *A Biomimetic Tumor Model of Heterogeneous Invasion in Pancreatic Ductal Adenocarcinoma.* Small, 2020. **16**(10): p. 1905500.
141. Huber, D., et al., *Hydrodynamics in cell studies.* Chemical reviews, 2018. **118**(4): p. 2042-2079.
142. Cross, V.L., et al., *Dense type I collagen matrices that support cellular remodeling and microfabrication for studies of tumor angiogenesis and vasculogenesis in vitro.* Biomaterials, 2010. **31**(33): p. 8596-8607.
143. Ng, C.P. and M.A. Swartz, *Fibroblast alignment under interstitial fluid flow using a novel 3-D tissue culture model.* American Journal of Physiology-Heart and Circulatory Physiology, 2003. **284**(5): p. H1771-H1777.
144. Park, S., et al., *Microstructural parameter-based modeling for transport properties of collagen matrices.* Journal of biomechanical engineering, 2015. **137**(6).
145. Van Haastert, P.J. and M. Postma, *Biased random walk by stochastic fluctuations of chemoattractant-receptor interactions at the lower limit of detection.* Biophysical journal, 2007. **93**(5): p. 1787-1796.
146. Fuller, D., et al., *External and internal constraints on eukaryotic chemotaxis.* Proceedings of the National Academy of Sciences, 2010. **107**(21): p. 9656-9659.
147. Ligorio, M., et al., *Stromal Microenvironment Shapes the Intratumoral Architecture of Pancreatic Cancer.* Cell, 2019. **178**(1): p. 160-175.e27.
148. Rofstad, E.K., K. Galappathi, and B.S. Mathiesen, *Tumor interstitial fluid pressure—a link between tumor hypoxia, microvascular density, and lymph node metastasis.* Neoplasia, 2014. **16**(7): p. 586-594.